Monthly Notices
of the
ROYAL ASTRONOMICAL SOCIETY

MNRAS **471,** 1709–1727 (2017) doi:10.1093/mnras/stx1710
Advance Access publication 2017 July 8

Not so lumpy after all: modelling the depletion of dark matter subhaloes by Milky Way-like galaxies

Shea Garrison-Kimmel,[1]★ Andrew Wetzel,[1,2,3]† James S. Bullock,[4] Philip F. Hopkins,[1] Michael Boylan-Kolchin,[5] Claude-André Faucher-Giguère,[6] Dušan Kereš,[7] Eliot Quataert,[8] Robyn E. Sanderson,[1] Andrew S. Graus[4] and Tyler Kelley[4]

[1]*TAPIR, California Institute of Technology, Pasadena, CA 91125, USA*
[2]*The Observatories of the Carnegie Institution for Science, Pasadena, CA 91125, USA*
[3]*Department of Physics, University of California, Davis, CA 95616, USA*
[4]*Center for Cosmology, Department of Physics and Astronomy, University of California, Irvine, CA 92697, USA*
[5]*Department of Astronomy, The University of Texas at Austin, 2515 Speedway, Stop C1400, Austin, TX 78712*
[6]*Center for Interdisciplinary Exploration and Research in Astrophysics (CIERA) and Department of Physics and Astronomy, Northwestern University, 2145 Sheridan Road, Evanston, IL 60208, USA*
[7]*Department of Physics, Center for Astrophysics and Space Sciences, University of California, San Diego, La Jolla, CA 92093 USA*
[8]*Department of Astronomy and Theoretical Astrophysics Center, University of California, Berkeley, CA 94720-3411, USA*

Accepted 2017 July 5. Received 2017 July 5; in original form 2017 January 17

ABSTRACT

Among the most important goals in cosmology is detecting and quantifying small ($M_{\rm halo} \simeq 10^{6-9}$ M$_\odot$) dark matter (DM) subhaloes. Current probes around the Milky Way (MW) are most sensitive to such substructure within ∼20 kpc of the halo centre, where the galaxy contributes significantly to the potential. We explore the effects of baryons on subhalo populations in ΛCDM using cosmological zoom-in baryonic simulations of MW-mass haloes from the Latte simulation suite, part of the Feedback In Realistic Environments (FIRE) project. Specifically, we compare simulations of the same two haloes run using (1) DM-only (DMO), (2) full baryonic physics and (3) DM with an embedded disc potential grown to match the FIRE simulation. Relative to baryonic simulations, DMO simulations contain ∼2 × as many subhaloes within 100 kpc of the halo centre; this excess is $\gtrsim$5 × within 25 kpc. At $z = 0$, the baryonic simulations are completely devoid of subhaloes down to 3×10^6 M$_\odot$ within 15 kpc of the MW-mass galaxy, and fewer than 20 surviving subhaloes have orbital pericentres <20 kpc. Despite the complexities of baryonic physics, the simple addition of an embedded central disc potential to DMO simulations reproduces this subhalo depletion, including trends with radius, remarkably well. Thus, the additional tidal field from the central galaxy is the primary cause of subhalo depletion. Subhaloes on radial orbits that pass close to the central galaxy are preferentially destroyed, causing the surviving population to have tangentially biased orbits compared to DMO predictions. Our method of embedding a potential in DMO simulations provides a fast and accurate alternative to full baryonic simulations, thus enabling suites of cosmological simulations that can provide accurate and statistical predictions of substructure populations.

Key words: galaxies: haloes – Local Group – dark matter – cosmology: theory.

1 INTRODUCTION

One of the strongest predictions of ΛCDM [cosmological constant with cold dark matter (DM)] is that DM clusters hierarchically: large haloes that host Milky Way (MW)-size galaxies are filled with smaller, self-bound clumps known as subhaloes. The highest-resolution cosmological simulations of MW-size haloes in the ΛCDM paradigm have demonstrated that DM clumps exist at all resolved masses (e.g. Springel et al. 2008; Kuhlen, Madau & Silk 2009; Stadel et al. 2009; Garrison-Kimmel et al. 2014a; Griffen et al. 2016).

★ E-mail: sheagk@caltech.edu
† Caltech-Carnegie Fellow.

While at least some of these subhaloes are presumed to host faint satellite galaxies, the 'missing satellites' problem (Klypin et al. 1999; Moore et al. 1999) points out a sharp discrepancy between the flat luminosity function of observed satellites and the steep, ever-rising mass function of subhaloes predicted from numerical simulations. Though the discrepancy can be largely eliminated by invoking gas heating from reionization suppressing star formation in the early Universe (Bullock, Kravtsov & Weinberg 2000; Somerville 2002) and observational incompleteness (Tollerud et al. 2008), this solution demands that subhaloes with bound masses smaller than $\sim 10^8\,\mathrm{M}_\odot$ should be *dark* and that thousands of $\sim 10^6\,\mathrm{M}_\odot$ subhaloes should be entirely devoid of stars.

Confirming the existence of these tiny, dark subhaloes, and further determining their mass function, would simultaneously provide an astounding confirmation of the ΛCDM theory and rule out large classes of warm DM models and inflationary models that predict a cut-off in the power spectrum at low masses (Kamionkowski & Liddle 2000; Bode, Ostriker & Turok 2001; Zentner & Bullock 2003; Bose et al. 2016; Bozek et al. 2016; Horiuchi et al. 2016). Because these subhaloes are dark, however, they must be identified indirectly. Around the MW, the best possibilities for detecting dark substructure are through perturbations to the stellar disc (e.g. Quinn, Hernquist & Fullagar 1993; Feldmann & Spolyar 2015, and references therein) and via gaps or kinematic distortions in dynamically cold stellar streams formed from disrupting globular clusters, such as Palomar-5 and GD-1 (e.g. Johnston, Spergel & Haydn 2002; Koposov, Rix & Hogg 2010; Carlberg, Grillmair & Hetherington 2012; Ngan et al. 2015, and references therein). In fact, Bovy, Erkal & Sanders (2017) recently claimed a measurement of 10^{+11}_{-6} subhaloes of mass 3×10^6–$3 \times 10^9\,\mathrm{M}_\odot$ within 20 kpc of the MW via the Palomar-5 stream. Amorisco et al. (2016), however, argued that giant molecular clouds could also be responsible for some of the fluctuations, and Ibata, Lewis & Martin (2016) reported a null detection using the same stream. Currently undetected stellar streams may provide more information about dark substructure around the MW (Ngan et al. 2016). Around larger, more distant galaxies, dark substructures may be revealed by gravitational lensing anomalies from background sources (Mao & Schneider 1998; Dalal & Kochanek 2002; Vegetti et al. 2010; MacLeod et al. 2013; Nierenberg et al. 2014; Hezaveh et al. 2016), particularly with the upcoming instruments on James Webb Space Telescope (JWST; MacLeod et al. 2013). These lensing studies are sensitive to substructure within a projected Einstein radius that is typically ∼5–10 kpc in size (Dalal & Kochanek 2002; Fiacconi et al. 2016).

Making predictions for these observations, and thus using them to constrain the properties of DM on small scales, requires a *statistical* sample of haloes simulated in ΛCDM with sufficient resolution (particle mass $\lesssim 10^5\,\mathrm{M}_\odot$) to identify the tiny subhaloes of interest. While several such simulations exist in the literature (e.g. Springel et al. 2008; Kuhlen, Madau & Silk 2009; Stadel et al. 2009; Mao, Williamson & Wechsler 2015; Griffen et al. 2016), the vast majority are purely collisionless (DM-only; DMO), given their low computational cost compared with fully baryonic simulations. However, DMO simulations are problematic because they miss critical baryonic physics, including the simple presence of a central galaxy in the halo, near the very regions where observational probes of substructure are most sensitive. While the smallest subhaloes are likely devoid of baryons, they nonetheless should be dynamically influenced by the central galaxy (Taylor & Babul 2001; Hayashi et al. 2003; Berezinsky, Dokuchaev & Eroshenko 2006; Read et al. 2006a,b; D'Onghia et al. 2010; Peñarrubia et al. 2010). In fact, the mere existence of a stellar halo around the MW implies a significant population of destroyed dwarf galaxies.

Furthermore, observational estimates for the masses of larger subhaloes, which host luminous dwarf galaxies and therefore can be identified through direct observations, are well below expectations from DMO simulations of MW-like haloes. The magnitude of this discrepancy, which is known as the 'too-big-to-fail' problem (Boylan-Kolchin, Bullock & Kaplinghat 2011, 2012; see also Tollerud, Boylan-Kolchin & Bullock 2014, for similar results for M31, and Garrison-Kimmel et al. 2014b; Papastergis et al. 2015, for field dwarf galaxies), depends on the adopted mass of the MW (di Cintio et al. 2011; Wang et al. 2012; Vera-Ciro et al. 2013), but internal baryonic processes (such as rapid gaseous outflows driven by bursty stellar feedback that can turn the cuspy DM profiles predicted by collisionless simulations into cored profiles with central masses at $r \lesssim 500$ pc that are consistent with the observations) appear important for resolving TBTF (e.g. Navarro, Frenk & White 1996; Read & Gilmore 2005; Mashchenko, Wadsley & Couchman 2008; Governato et al. 2012; Pontzen & Governato 2012; Gritschneder & Lin 2013; Amorisco, Zavala & de Boer 2014; Chan et al. 2015; Oñorbe et al. 2015). As Brooks & Zolotov (2014) showed, the increased tidal forces from the central galaxy also can reduce the central masses of such dwarf galaxies even further, potentially eliminating the disagreement between theory and observations entirely (see also Read et al. 2006a,b). Additionally, the central galaxy potential may completely destroy some of the large, dense subhaloes, effectively lowering theoretical predictions for the central masses of the haloes expected to host the luminous dwarfs by placing them in correspondingly lower mass, and thus more abundant, subhaloes (see also Garrison-Kimmel et al. 2017). However, the amount of destruction that can be unambiguously attributed to the central galaxy remains uncertain.

Recently, the 'Latte' simulation (Wetzel et al. 2016), part of the Feedback In Realistic Environments (FIRE) project, achieved baryonic mass resolution of $\sim 7000\,\mathrm{M}_\odot$ for a MW-mass halo run to $z = 0$. The Latte simulation resolves subhaloes down to mass $\sim 10^6\,\mathrm{M}_\odot$, and as Wetzel et al. (2016) showed, the initial Latte simulation produces a population of satellite dwarf galaxies that agrees with a wide variety of observations around the MW and M31: the distributions of stellar masses, velocity dispersions, and star formation histories, and the relationship between stellar mass and metallicity all agree well with those of the MW satellites. Thus, it does not suffer from either the missing satellites or too-big-to-fail problems, at least for resolved satellite dwarf galaxies ($M_\star \gtrsim 10^5\,\mathrm{M}_\odot$). Using the APOSTLE simulations of Local Group-like MW-M31 pairs, Sawala et al. (2017) also recently found good observational agreement for satellite stellar masses and subhalo circular velocities using different treatments of baryonic physics. While these results from baryonic simulations are quite promising, such simulations are sufficiently expensive to prohibit large parameter surveys and statistical samples.

In this work, we extend the initial analysis of Wetzel et al. (2016) to study substructure populations down to the smallest mass scales of relevance for current dark substructure searches ($\sim 10^6\,\mathrm{M}_\odot$). We also present a second simulation of a MW-mass galaxy in the Latte suite. We will show that properly accounting for the effects of baryons is essential for accurately predicting subhalo populations, even for completely dark subhaloes that have no stars. Motivated by previous work that suggested that adding an analytic potential or other inexpensive modification(s) to DMO simulations could capture the key baryonic effects on dark subhaloes (e.g. D'Onghia et al. 2010; Jethwa, Belokurov & Erkal 2016; Zhu et al. 2016;

Table 1. Properties of the two host haloes, `m12i` (first presented in Wetzel et al. 2016) and `m12f` (first presented here and to be presented in more detail in Wetzel et al., in preparation). '`-dmo`' refers to a DM-only (DMO) simulation of the same halo, while '`-disk`' indicates a DM + embedded disc potential simulation; the entries without an appendix represent the FIRE baryonic simulations. The '$2M_{\rm d}$', '$M_\star + M_{\rm gas}$', '$2R_{\rm d}$', '$z_{\rm d}0$' and '`Hernquist`' simulations below the break indicate runs discussed in Section 3.4, which include factors of $\lesssim 2$ changes to the disc parameters, or, in the final case, a spherically symmetric potential with the same mass. The columns indicate the name of the simulation, the mass of the host halo (using the virial definition of Bryan & Norman 1998), the maximum circular velocity, $V_{\rm max}$, of the host halo (including only DM), the virial velocity, $V_{\rm v}$, of the host halo (defined as $\sqrt{GM_{\rm v}/R_{\rm v}}$, where $R_{\rm v}$ is the virial radius), the number of subhaloes within 25, 50, 100 and 300 kpc at $z = 0$ with $V_{\rm max} > 5\,{\rm km\,s^{-1}}$ (corresponding roughly to $M_{\rm bound} \simeq 5 \times 10^6\,{\rm M_\odot}$), and $f_{\rm bound}$, the total mass in resolved subhaloes divided by the virial mass of the host. $M_{\rm v}$ and $V_{\rm v}$ for the baryonic simulations include the contributions of gas and stars. However, we list $V_{\rm max}$ based only on DM for these runs because the circular velocity curve peaks at small radii ($r \simeq 1.6$ kpc) when including baryons in the mass profile; in this case, `m12i` reaches $V_{\rm max} = 279\,{\rm km\,s^{-1}}$ while `m12f` reaches $V_{\rm max} = 283\,{\rm km\,s^{-1}}$.

Simulation	$M_{\rm v}$ ($10^{12}\,{\rm M_\odot}$)	$V_{\rm max}$ (km s^{-1})	$V_{\rm v}$ (km s^{-1})	$N_{\rm sub}$ (<25 kpc)	$N_{\rm sub}$ (<50 kpc)	$N_{\rm sub}$ (<100 kpc)	$N_{\rm sub}$ (<300 kpc)	$f_{\rm bound}$
`m12f`	1.6	183	149	4	62	266	1482	0.037
`m12f-dmo`	1.6	177	150	42	204	654	2423	0.081
`m12f-disk`	1.7	195	153	13	97	379	1854	0.049
`m12i`	1.1	163	134	9	57	370	1432	0.056
`m12i-dmo`	1.1	162	134	39	200	671	2069	0.078
`m12i-disk`	1.2	191	136	6	108	473	1712	0.062
`m12i-disk-`$2M_{\rm d}$	1.2	220	138	5	96	455	1619	0.051
`m12i-disk-`$M_\star + M_{\rm gas}$	1.2	188	136	9	45	352	2142	0.062
`m12i-disk-`$2R_{\rm d}$	1.2	189	136	16	129	485	1738	0.062
`m12i-disk-`$z_{\rm d}0$	1.2	183	136	19	120	529	1733	0.061
`m12i-Hernquist`	1.2	216	136	10	70	385	2214	0.066

Errani et al. 2017; Sawala et al. 2017), we apply a method for inserting an approximate analytic description of the gravitational potential of the galaxy that forms at the centre of each MW-mass halo into a cosmological DMO simulation.

Our approach is particularly interesting for testing the underlying physical drivers, because we both calibrate our input central disc model and benchmark our results against our fully baryonic simulations, which reproduce many observable properties of the satellite populations around the MW and M31. As we will show, many key differences in subhaloes populations between DMO and baryonic simulations can be unambiguously attributed to the presence of the central galaxy potential. This success of embedding a central galaxy potential also demonstrates that the substructure populations predicted by cosmological DMO simulations can be significantly improved (i.e. brought into better agreement with fully baryonic simulations) at minimal CPU cost.

In Section 2, we discuss the simulations and detail our method of inserting an embedded potential into the centre of the host; Section 3 explores subhalo population statistics with and without a forming galaxy and presents trends with a radius in subhalo depletion. We discuss further implications of our results in Section 4 and conclude in Section 5.

Throughout this work, we use $h = 0.702$, $\Omega_{\rm m} = 0.272$, $\Omega_{\rm b} = 0.0455$ and $\Omega_\Lambda = 0.728$.

2 SIMULATIONS

All of our simulations are cosmological and employ the 'zoom-in' technique (Katz & White 1993; Oñorbe et al. 2014). We run all of our simulations in the same cosmological volume as the AGORA project (Kim et al. 2014), with a box length of $60h^{-1}$ Mpc $= 85.5$ Mpc. We choose each high-resolution region to contain a single MW-mass ($M_{\rm halo} \sim 10^{12}\,{\rm M_\odot}$) halo at $z = 0$ that has no neighbouring haloes of similar or greater mass within 3 Mpc. We focus on two such haloes, designated as `m12i` and `m12f`, which are part of the Latte sample from the FIRE project. `m12i` was presented in Wetzel et al. (2016); `m12f` was simulated with identical parameters using the same pipeline and will be described in detail in Wetzel et al. (in preparation). We chose both haloes based only on their virial mass (see Table 1) and not based on their formation/merger history or subhalo population.

We ran all simulations using GIZMO (Hopkins 2015),[1] which uses an updated version of the TREE+PM gravity solver included in GADGET-3 (Springel 2005). We identify halo centres and create halo catalogs with `AHF` (Knollmann & Knebe 2009) and build merger trees using `consistent-trees` (Behroozi et al. 2013a). We generated initial conditions for the DMO and baryonic simulations at $z = 100$ using `MUSIC` (Hahn & Abel 2011) with second-order Lagrangian perturbation theory. For the embedded disc simulations, we generated initial conditions using the snapshot at $z = 3$ from the DMO simulations.

The properties of the two host haloes, along with the number of resolved subhaloes identified by `AHF` within several radial cuts of that host, are listed in Table 1. The first column lists the names of the simulations: those identified with '`dmo`' are purely collisionless, while the simulations labeled as '`disk`' are DMO with an embedded galactic potential; the other rows show the FIRE baryonic simulations. The remaining columns list the Bryan & Norman (1998) virial masses, maximum circular velocities, $V_{\rm max}$, and virial velocities ($\sqrt{GM_{\rm v}/R_{\rm v}}$) of the hosts, here calculated from the full particle distribution (including gas and stars in the baryonic simulations), the total number of subhaloes with $V_{\rm max} > 5\,{\rm km\,s^{-1}}$ that survive to $z = 0$ within 25, 50, 100 and 300 kpc of the halo centre, and the fraction of the host mass that resides in self-bound subhaloes.

2.1 Baryonic simulations

The baryonic simulation of `m12i` analysed here is the same run presented in Wetzel et al. (2016); `m12f` was simulated with an identical code and parameters. The physics and numerical prescriptions are

[1] http://www.tapir.caltech.edu/~phopkins/Site/GIZMO.html

therefore given in Wetzel et al. (2016). Briefly, however, the baryonic simulations are part of the Feedback In Realistic Environments (FIRE; Hopkins et al. 2014) project.[2] Specifically, they use the updated FIRE-2 code, which features identical physics as FIRE-1 but incorporates several *numerical* improvements. In particular, FIRE-2 adopts the new mesh-free finite mass method for more accurate hydrodynamics (Hopkins 2015). We model radiative heating and cooling from 10 to 10^{10} K (following CLOUDY tabulations; Ferland et al. 1998), and accounting for self-shielding and photo-heating both by an ultraviolet (UV) background (from Faucher-Giguère et al. 2009) and by local sources. Star formation occurs in self-gravitating gas (according to the criterion in Hopkins, Narayanan & Murray 2013) that is also molecular and self-shielding (following Krumholz & Gnedin 2011), Jeans unstable, and exceeds a minimum density threshold $n_{\rm sf} > 1000\,{\rm cm}^{-3}$. A star particle is then spawned probabilistically from a gas particle, inheriting the same mass and metallicity. The simulations follow several stellar feedback mechanisms, including (1) local and long-range momentum flux from radiation pressure (in the initial UV/optical single-scattering, and from re-radiated light in the IR), (2) energy, momentum, mass and metal injection from core-collapse and Ia supernovae, as well as stellar mass loss from OB and AGB stars, and (3) photoionization and photoelectric heating. Every star particle is treated as a single stellar population with a mass, age and metallicity. We tabulate all feedback event rates, luminosities and energies, mass-loss rates, and other quantities directly from stellar evolution models (STARBURST99 v7.0; Leitherer et al. 1999) assuming a Kroupa (2001) initial mass function.

Full details of FIRE-2 are provided in Hopkins et al. (2017). The source code and numerical parameters of our baryonic simulations are *exactly* identical to those in all FIRE-2 simulations (Fitts et al. 2016; Su et al. 2016; Wetzel et al. 2016).

The FIRE simulations have been shown to reproduce a wide variety of observables, including the relationships between stellar mass and halo mass, the Kennicutt–Schmidt law, bursty star formation histories, the star-forming main sequence (Hopkins et al. 2014), galactic winds (Muratov et al. 2015, 2017), the gas and stellar phase $M_\star$-metallicity relations (Ma et al. 2016), the $M_\star$-size relation (El-Badry et al. 2016), the HI content of galaxy haloes at both low and high redshift (Faucher-Giguère et al. 2015, 2016; Hafen et al. 2017) and the structure and star formation histories of isolated dwarf galaxies (Chan et al. 2015; Oñorbe et al. 2015; Fitts et al. 2016). Moreover, in simulations of MW-mass haloes, in addition to forming a realistic MW-like galaxy in terms of stellar mass and disc morphology (Wetzel et al. 2016; Ma et al. 2017), the FIRE model yields reasonable populations of dwarf galaxies around those galaxies, in terms of the distributions of stellar masses and velocity dispersions, as well as a wide range of star formation histories that agree well with those of the actual MW satellites.

Both `m12i` and `m12f` form thin, radially extended stellar discs with $M_\star(R < R_{90}, z < z_{90}) = 6.2 \times 10^{10}\,{\rm M}_\odot$ and $7.5 \times 10^{10}\,{\rm M}_\odot$, respectively, where R_{90} and z_{90} are the radius and height that contain 90 per cent of the mass. Thus, these galaxies are comparable to, if slightly more massive than, the MW in stars (Bland-Hawthorn & Gerhard 2016). At $z = 0$, the total gas fraction, $M_{\rm gas}/(M_\star + M_{\rm gas})$, within R_{90} and z_{90} is 13 per cent for `m12i` and 15 per cent for `m12f`.

The gravitational force softenings and kernel smoothing lengths for gas particles are fully adaptive and conservative (following Price & Monaghan 2007). Hydrodynamic smoothings and gravitational force softenings are always self-consistently matched. The minimum gas smoothing/Plummer equivalent softening achieved in both simulations is $\epsilon_{\rm gas,\,min} = 1\,{\rm pc}$ (corresponding to a density of $n_{\rm gas} \approx 10^7\,{\rm cm}^{-3}$), thus ensuring that dense, star-forming regions are well resolved. We choose softenings for the DM particles to be comparable to the typical gas softening in the host galaxy's disc: $\epsilon_{\rm DM} = 20\,{\rm pc}$. The softenings for the stars are $\epsilon_{\rm stars} = 8\,{\rm pc}$, chosen to match the gas softening at the density threshold for star-forming regions, $n_{\rm sf} > 1000\,{\rm cm}^{-3}$. All (minimum) softening lengths quoted here are fixed in physical units after $z = 9$, and evolve co-moving with the scale factor prior to that redshift. Each simulation is initialized at an 'effective' resolution of 2×8192^3 particles within the box, resulting in a DM particle mass of $m_{\rm DM} = 3.5 \times 10^4\,{\rm M}_\odot$ and a (initial) gas or star particle mass of $m_{\rm gas} = 7.1 \times 10^3\,{\rm M}_\odot$.

2.2 DM-only simulations

The DMO simulations are identical to the baryonic simulations, except that they include only DM particles, and the baryonic mass is included in the DM particles. Consequently, the particle masses are larger by a factor of $1/(1 - f_{\rm b})$, where $f_{\rm b} = \Omega_b/\Omega_{\rm m} \simeq 0.17$ is the cosmic baryon fraction: $m_{\rm DM,\,DMO} = 4.2 \times 10^4\,{\rm M}_\odot$. This increased particle mass has non-trivial effects on comparisons of DMO and baryonic simulations, both directly, as in the case of subhalo mass functions, and indirectly, through implied resolution cuts. This difference is particularly relevant for low-mass subhaloes, which have lost essentially all of their baryonic mass by $z = 0$ from cosmic re-ionization, feedback-driven gas heating, and ram-pressure stripping within the host halo. Thus, a given subhalo may contain an identical number of DM particles in the collisionless and baryonic simulations, but be more massive in the former. Therefore, for low-mass subhaloes, which are expected to have lost (nearly) all of their baryonic mass, the most physical way to quote their masses in DMO simulations is to correct for this (presumed) baryonic mass loss. We thus multiply all particle and subhalo masses by $1 - f_{\rm b}$ in all post-processing (after halo finding), and we similarly suppress the maximum circular velocities of all subhaloes $V_{\rm max}$ by $\sqrt{1 - f_{\rm b}}$ (similar to Zolotov et al. 2012). Finally, we perform halo finding only on the DM particles in the baryonic simulations, to achieve the fairest comparison. Therefore, the differences between baryonic and DMO simulations that we quote here are somewhat smaller than those quoted in Wetzel et al. (2016), who did not include this correction.

2.3 Embedded disc potentials

To include the effects of the disc of the central galaxy – which grows naturally within baryonic simulations – in our DMO simulations, we add an additional gravitational acceleration to every particle active during each timestep, as given by a Miyamoto & Nagai (1975) potential:

$$\Phi(R, z) = \frac{G M_{\rm d}}{\left\{ \Delta R^2 + \left[R_{\rm d} + \left(\Delta z^2 + z_{\rm d}^2 \right)^{1/2} \right]^2 \right\}^{1/2}}, \quad (1)$$

where ΔR and Δz indicate the relative position from the centre of the potential $(x_{\rm disc}, y_{\rm disc}, z_{\rm disc})$ in cylindrical coordinates: $\Delta R^2 = (x - x_{\rm disc})^2 + (y - y_{\rm disc})^2$; $\Delta z^2 = (z - z_{\rm disc})^2$. This potential has three parameters: $R_{\rm d}(z)$, the disc scale length, $z_{\rm d}(z)$, the disc scale height, and $M_{\rm d}(z)$, the total mass in the potential.

[2] http://fire.northwestern.edu

Importantly, the acceleration from the Miyamoto–Nagai disc is analytic: in the plane of the disc, taken here to be the x–y plane, it is

$$a_x = \frac{-GM_{\rm d}}{\left\{\Delta R^2 + \left[R_{\rm d} + \left(\Delta z^2 + z_{\rm d}^2\right)^{1/2}\right]^2\right\}^{3/2}} \Delta x, \quad (2)$$

where $\Delta x = (x - x_{\rm disc})$, and similarly in the y direction. The acceleration along the minor axis, taken to be the z direction, is

$$a_z = \frac{-GM_{\rm d}\left[R_{\rm d} + \left(\Delta z^2 + z_{\rm d}^2\right)^{1/2}\right]}{\left\{\Delta R^2 + \left[R_{\rm d} + \left(\Delta z^2 + z_{\rm d}^2\right)^{1/2}\right]^2\right\}^{3/2} \left(\Delta z^2 + z_{\rm d}^2\right)^{1/2}} \Delta z. \quad (3)$$

Within the DMO simulation, we track the centre of the MW-mass host halo across cosmic time using a single massive ($m_{\rm p} = 10^8\,{\rm M}_\odot/h$) particle inserted at the centre of the main branch of the host at $z = 3$, using a large softening length ($\epsilon = 3.7$ physical kpc). This effectively acts as a small bulge in the centre of the galaxy. Because this particle is significantly more massive than the high-resolution particles that comprise the remainder of the halo, dynamical friction acts to keep it near the centre of the host.[3] The position of this particle at each timestep determines the centre of the disc potential. To minimize computational cost, (x, y, z) offsets from this particle are computed for all other particles while traversing the gravity tree.

In our embedded disc simulations, we allow this disc potential to evolve over time to match the stellar disc that forms in the corresponding baryonic simulation of the same system. We first embed the disc potential at $z = 3$ ($\sim$11.5 Gyr ago), initializing with parameters ($M_{\rm d}$, $R_{\rm d}$ and $z_{\rm d}$) obtained by jointly fitting the average density profile of each baryonic simulation's stellar disc along the major and minor axes, defined by solving for the eigenvectors of the moment of inertia tensor of all stars within 20 kpc. We then linearly interpolate each parameter in a scale factor between fits performed at 12 additional snapshots, equally spaced in z, to $z = 0$. In all fits, we bound the total mass in the potential to be less than 0.1 dex greater than the stellar mass of the disc in the baryonic simulation. This method yields an excellent match between the stellar mass in the baryonic simulations and the mass in the embedded discs within fixed physical radii.[4]

Table 2 lists the physical parameters of the analytic disc potential, and equivalent quantities for the galaxies that form in the FIRE simulations. The first two columns quote the mass, quantified as $M_{\rm d}$ for the disc potential (the total mass when integrated to infinity) and by $M(<r_{90})/0.9$ for the FIRE simulations, where r_{90} is the 3D radius that contains 90 per cent of the mass. The last two columns give the radial extent of the disc, quantified here by the 2D radius R_{90}, where $M(R < R_{90}) = 0.9 \times M(z < z_{90})$ and z_{90} similarly contains 90 per cent of the total stellar mass of the galaxy.

While we carefully design the analytic potential to match the parameters of the stellar disc in the baryonic simulations, we note several limitations. For simplicity, we fix the orientation of the disc to be along the x–y-axis plane (rather than allowing it to rotate through arbitrary angles). Additionally, in the baryonic simulations, `m12i` and `m12f` do not form permanent well-ordered discs until $z \approx 0.5$ and $z \approx 0.6$, respectively, so our assumed potential overestimates the thinness of the disc at early times. However, as we show below, the 'thinness' of the disc is not important for capturing its tidal effects on subhaloes – in fact, replacing the disc with a *spherical* Hernquist (1990) profile of the same mass produces nearly the same effect (see Section 3.4). Furthermore, we add this disc potential to the DMO simulation without adjusting the mass of DM particles, thus slightly increasing the overall mass within the host halo. However, this error is likely small to the overall system because the discs comprise only $\sim$6 per cent of the total mass within $R_{\rm v}$ and 10 per cent within 80 kpc.

We also fit our fiducial discs to only the stellar mass from the baryonic simulation; we do not try to fit the gaseous component. This is a reasonable approximation at $z = 0$, where the gas fractions in the discs of our simulated host galaxies are $\approx$15 per cent, comparable to the MW, M31, and similar galaxies (Yin et al. 2009; Catinella et al. 2010, 2012, 2013). At higher redshifts, however, when the discs were more gas-rich, our method underestimates the total baryonic mass within the disc. At these redshifts, stellar feedback drives significant gas flows in and out of galaxy on short time-scales ($\lesssim$100 Myr), compromising the accuracy of any simple, constant analytic description of the resultant potential. In principle, this lack of incorporating gas implies that our stellar-disc-only model represents a lower limit to the level of substructure depletion from the central galaxy, though, as we show in Section 3.4 by increasing the mass of the embedded disc to include the gas in the galaxy, the purely gravitational contribution from gas is small.

However, as we demonstrate below, even this simple model is remarkably successful at reproducing the statistical properties of surviving subhaloes as compared with the fully baryonic simulations. Thus, while there is room for further progress, our method represents a *substantial* improvement over DMO simulations at essentially the same CPU cost.

Table 2. Properties of the analytic 'embedded disc' of the MW-mass central galaxies at several redshifts, along with the properties from the FIRE baryonic simulations that we model the discs on. The first two columns list the total mass in the embedded disc, $M_{\rm d}$, and the equivalent stellar mass in the FIRE galaxy; the following two columns list the radial extent of the disc (see the text for details). Our analytic discs are typically slightly more compact, particularly at late times, both because the Miyamoto–Nagai potential is an imperfect fit to the galaxies that form in the baryonic simulations and because we fit the density profile, rather than the mass or the potential. As we show in Section 3.4, the amount of substructure depletion most strongly depends on the disc mass; doubling $R_{\rm d}$ only weakly affects the surviving subhalo population.

	Redshift	$M_{\rm d}$ $10^{10}\,{\rm M}_\odot$	$M_{\rm gal}$ $10^{10}\,{\rm M}_\odot$	$R_{90,\,\rm disc}$ kpc	$R_{90,\,\rm gal}$ kpc
`m12i`	$z = 3$	0.09	0.12	15.75	14.86
	$z = 2$	0.32	0.29	15.84	12.57
	$z = 1$	1.59	1.44	7.94	10.76
	$z = 0.5$	4.28	3.91	4.22	5.93
	$z = 0$	8.56	7.70	6.43	9.49
`m12f`	$z = 3$	0.15	0.16	9.33	7.70
	$z = 2$	0.71	0.73	6.84	7.43
	$z = 1$	2.40	2.18	4.11	7.05
	$z = 0.5$	4.86	4.41	4.31	9.01
	$z = 0$	10.41	9.39	7.22	10.48

[3] At $z = 0$, the particle is within 12 pc of the centre of `m12i` found by `AHF` and within 235 pc of `m12f`, even without including the particle in the halo finding.

[4] At the 13 steps that anchor the time evolution, the disc potential matches the stellar mass within 20 kpc to within 10 per cent in `m12f` and within 20 per cent in `m12i` at worst; the average agreement over those 13 steps is $\sim$7 per cent across both simulations.

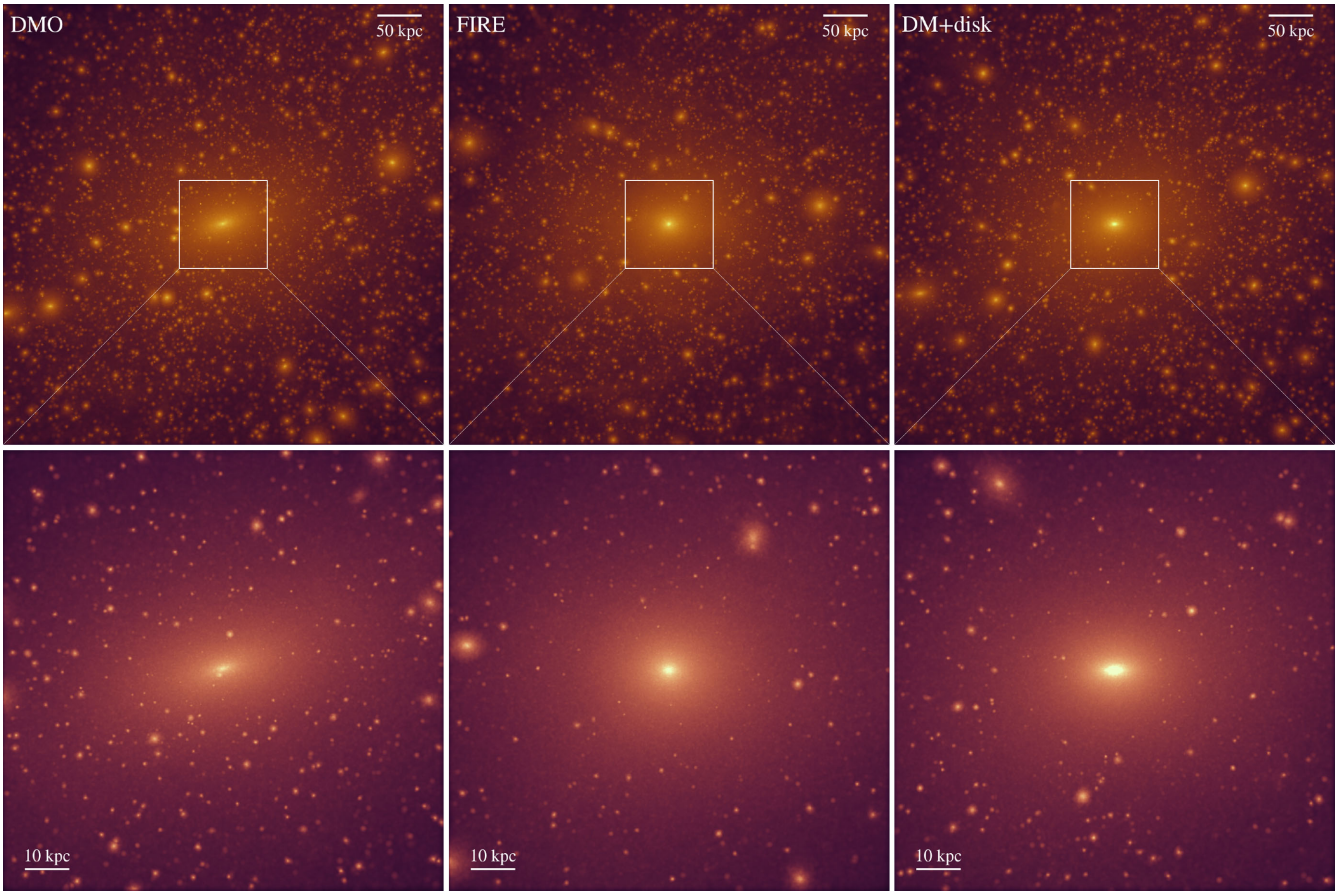

Figure 1. Visualizations of DM in the Latte `m12i` halo. Colouring indicates $\log_{10}$ of the local DM density. From left to right, the columns show the DM-only (DMO) simulation, the fully baryonic simulation using FIRE physics, and the DM-only run that adds an analytic, embedded disc potential to the halo centre (DM+disc), where the disc properties are matched to the baryonic simulation. The top row illustrates a cube 500 kpc on a side, while the bottom row zooms in on a cube 100 kpc across. The presence of the central galaxy (either real or embedded) leads to an enhancement in the DM density at the centre. Substructure counts are roughly similar on large scales in all cases (top row), but the tidal field of the central galaxy eliminates many subhaloes within ∼50 kpc (bottom row). Although the embedded disc potential does not capture all of the effects of baryons, it does effectively capture subhalo depletion in the inner halo, where searches for dark substructure via lensing or stellar streams are most sensitive. We quantify these differences in Figs 2–3.

3 RESULTS

Fig. 1 shows images of DM in our three types of simulations, highlighting the qualitative effect of the central galaxy on the DM distribution relative to the DMO simulation. The top panels visualize, from left to right, the DM density within a cube 500 kpc on a side in the DMO, FIRE baryonic, and embedded disc simulations of `m12i`; the lower panels show a zoomed-in view of a cube 100 kpc across. The log-scaled colour map changes from the upper to lower panels, but is identical across the simulations. The DM near the central galaxies (lower panels) clearly responds to the extra mass present in both the baryonic and embedded disc simulations. However, the DM takes on a slightly more disk-like shape around the analytic embedded potential; we posit that the relatively spherical cusp around the central galaxy in the baryonic simulation arises because of the continually evolving orientation of the central stellar disc, along with the fluctuating gas distribution, which is more spherical in a time-average sense because of time-dependent gas inflows and outflows.

Even more striking than the enhancement in the central DM density, however, is the *severe* reduction in the number of subhaloes within the central $r \lesssim 50$ kpc. The central galaxy has destroyed an enormous fraction of the satellites that the DMO simulation predicts in the central regions, where observational probes are most sensitive.

3.1 Dependence on mass and radius at $z = 0$

Fig. 2 quantifies the differences in the subhalo populations. The top row shows the cumulative counts of subhaloes within 100 kpc of `m12i` (left) and `m12f` (right) as a function of $V_{\rm max}$. The lower sub-panels show the ratio between the cumulative counts in the collisionless simulations (with and without the embedded potential) and the FIRE baryonic simulations. The DMO simulations, plotted in thin dashed lines, overpredict the subhalo $V_{\rm max}$ function relative to the baryonic simulations, plotted as solid lines, at all $V_{\rm max}$. The light dashed lines, which plot counts in the DMO simulations without correcting for the difference in particle masses between DMO and baryonic simulations, show that DMO predictions improve relative to the FIRE simulations after correcting for this effect, but only slightly – the disc reduces counts at fixed $V_{\rm max}$ by much more, particularly in `m12f`. In fact, the embedded disc simulations provide a significantly better match to the FIRE baryonic simulations at all $V_{\rm max}$. As demonstrated in the bottom panels, the disc simulations

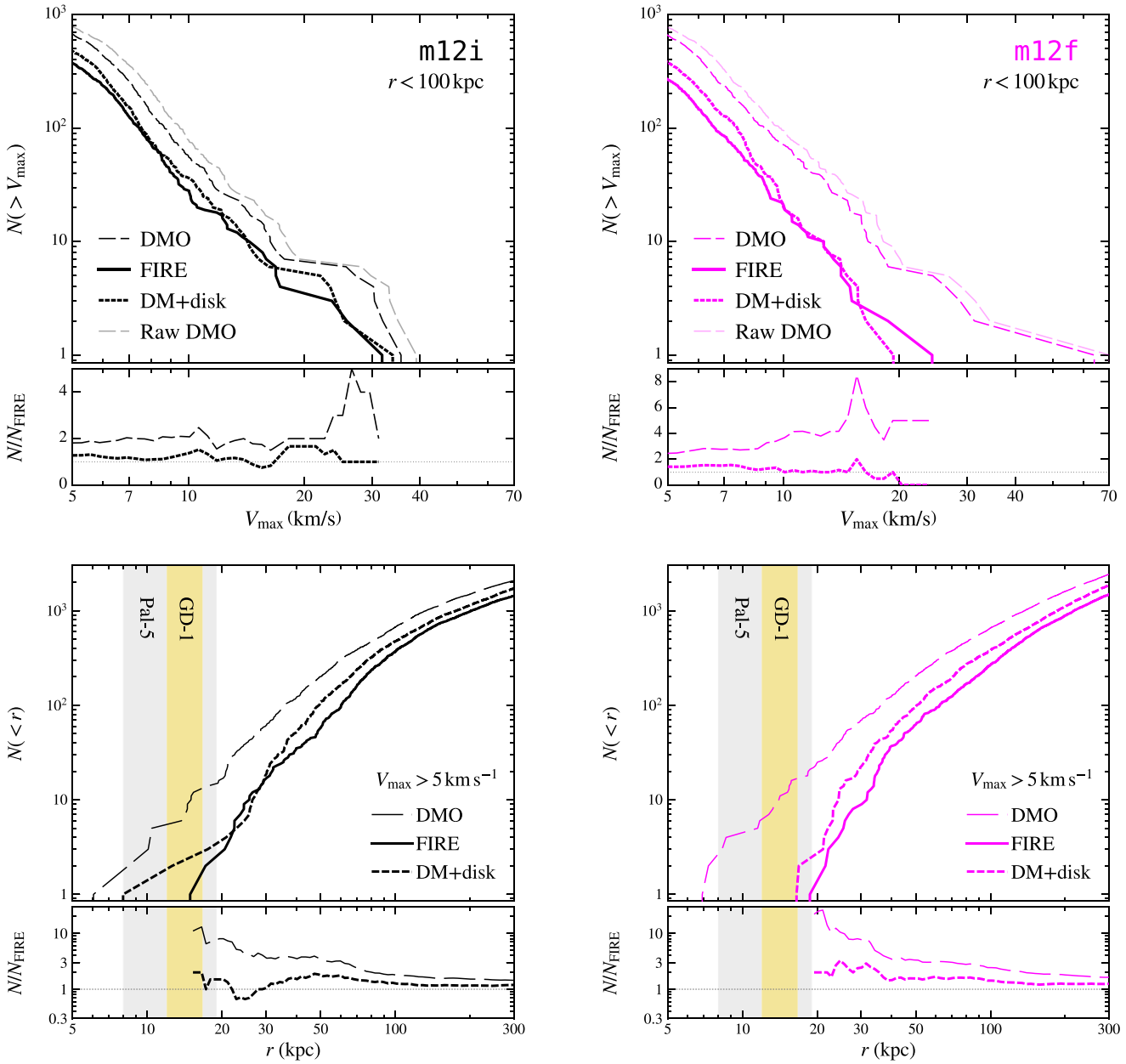

Figure 2. Top: Cumulative counts of subhaloes above a given maximum circular velocity, $V_{\rm max}$, within 100 kpc of the two hosts, `m12i` (left) and `m12f` (right) – Appendix A presents the counts within 50 and 300 kpc. For reference, the upper-most, light-coloured dashed lines (labeled 'Raw DMO') indicate the results of the DMO simulations *without* applying the correction for the baryon fraction (i.e. without multiplying by $\sqrt{1-f_{\rm b}}$). Henceforth we apply this correction for all comparisons. Lower panels plot the ratio between the cumulative counts of subhaloes in the DMO or embedded disc runs to the FIRE baryonic simulations. For both systems, the DMO simulation overpredicts the number of subhaloes as compared with the baryonic simulation by at least 2× at all $V_{\rm max}$: the average ratios plotted in the lower panels are 2.2 and 3.9 in `m12i` and `m12f`, respectively. Adding *only* the galactic disc potential brings the substructure counts to within ∼20 per cent agreement at all $V_{\rm max}$ (average ratios of 1.2 and 1.06). Bottom: Cumulative counts of subhaloes within a given radius. We include subhaloes down to $V_{\rm max} = 5\,{\rm km\,s^{-1}}$ (bound mass $M \simeq 5 \times 10^6\,{\rm M}_\odot$), which are well-resolved. While the total excess of subhaloes within 300 kpc $\approx R_{\rm vir}$ is ≈50 per cent in the DMO simulations, this excess rises to ≈3× within 50 kpc. Moreover, the disc *completely* destroys all subhaloes that are within 17–20 kpc by $z = 0$, where searches for dark substructure through stream heating are most sensitive: the light grey and gold bands show the extent of the galactocentric orbits of Palomar-5 (Carlberg et al. 2012) and GD-1 (Koposov et al. 2010), respectively, the best-studied streams around the MW. The embedded disc simulations model this reduction/destruction to within a factor of 2 at all radii. As we show in Section 3.3, ∼20 subhaloes with pericentric distances <20 kpc survive to $z = 0$.

agree with the baryonic simulations to within ∼20 per cent at nearly all $V_{\rm max}$.

The bottom row in Fig. 2 illustrates the radial distribution of the subhaloes included in the top row by showing the cumulative number of subhaloes as a function of 3D distance from the halo centre, r. As expected, the depletion is greatest at the centre of the host: both the `m12i` and `m12f` baryonic simulations have *no* subhaloes within 15 kpc and only 1–2 within 20 kpc at $z = 0$, while the DMO simulations predict ∼7 subhaloes within 15 kpc and $\gtrsim$10 within 20 kpc (see also Table 1). The embedded potential captures this effect

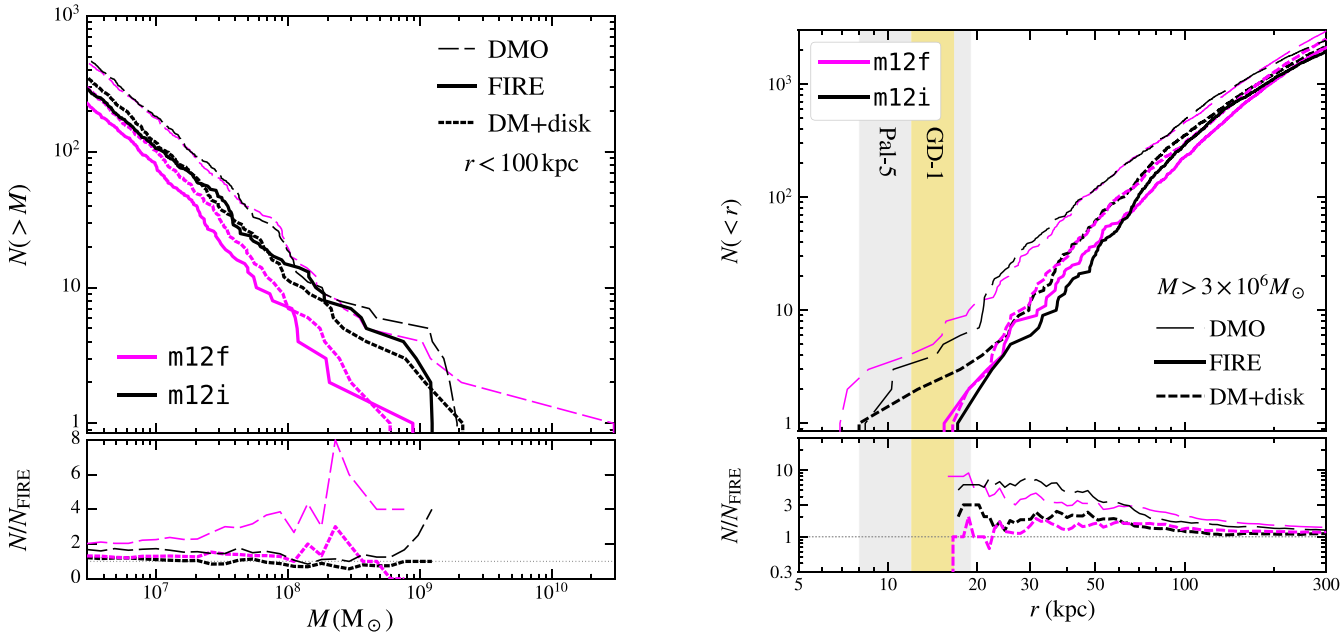

Figure 3. Cumulative number of subhaloes above a given bound DM mass, M, within 100 kpc (left) and as a function of radius, r, for $M > 3 \times 10^6\,\mathrm{M}_\odot$ (right). Lower panels plot the ratio between the cumulative counts of subhaloes in the DMO or embedded disc runs relative to the FIRE baryonic simulations. Selecting subhaloes via M instead of $V_{\rm max}$ (as in Fig. 2) leads to nearly identical results: DMO simulations overpredict the number of subhaloes as compared with the baryonic simulations at all M and r, while the embedded disc simulations show much better agreement.

well, particularly around m12f: only two subhaloes remain within 20 kpc. The match is slightly worse around m12i, where three subhaloes remain within 20 kpc and two subhaloes within 15 kpc, but the embedded disc simulation still improves upon the DMO simulation by a factor of ∼3. Though we do not explicitly plot it here, we also note that, even after accounting for the increased destruction via the disc, the radial distributions of the surviving subhaloes are more extended than predicted from DMO simulations.

This dearth of substructure within ∼20 kpc has strong implications for attempts to discover dark subhaloes via stellar streams around the MW. Thus far, the best-studied streams, Palomar 5 at 19 kpc (indicated by the grey vertical band; Carlberg et al. 2012) and GD-1 at ∼15 kpc (plotted as the gold band; Koposov et al. 2010), are within this distance, suggesting that baryonic simulations predict far fewer gaps in stellar streams than DMO simulations. The null result from Ibata et al. (2016) therefore may be in line with predictions from ΛCDM *including baryonic effects*. However, those gaps could be created by subhaloes at an earlier point in their orbits than their positions at $z = 0$; we therefore examine the distribution of pericentric distances $d_{\rm peri}$ in Section 3.3.

While $V_{\rm max}$ can be measured robustly in simulations, the degree to which a subhalo disrupts a stellar stream is more closely related to its bound mass (along with the interaction distance and velocity; e.g. Yoon, Johnston & Hogg 2011; Carlberg 2013; Sanders, Bovy & Erkal 2016; Sanderson et al. 2016). Therefore, the left-hand panel of Fig. 3 plots the cumulative subhaloes count, again within 100 kpc, as a function of the bound mass assigned to them by AHF, M. Because we run AHF only on DM particles, M therefore represents the bound DM mass. The results are similar to those using $V_{\rm max}$ as in Fig. 2, though the discrepancies between the DMO and baryonic simulations are less severe: the DMO simulations overpredict subhalo counts above fixed M by a factor of $\gtrsim$1.7.

The right-hand panel of Fig. 3 plots the cumulative radial distribution of subhaloes with $M > 3 \times 10^6\,\mathrm{M}_\odot$, which are reliably resolved in our simulations with 85 particles (Appendix B presents an explicit resolution test). The distributions are again similar to those in the lower plots in Fig. 2: simulations with a central galaxy predict only 1–3 subhaloes in the central 20 kpc, while the DMO simulations overpredict that count by a factor of >5. Therefore, the lack of substructure near the galaxy is independent of whether subhaloes are selected by $V_{\rm max}$ or M.

Because correcting for the reduction in the particle mass from the lack of baryons is more straightforward for M than for $V_{\rm max}$, which depends on the mass *profile* of the subhalo, we select subhaloes based on M for the remainder of the paper, using the resolution cut of $M > 3 \times 10^6\,\mathrm{M}_\odot$.

In general, the differences between the DMO and FIRE baryonic simulations are the largest among the most massive subhaloes ($V_{\rm max} \gtrsim 25\,\mathrm{km\,s^{-1}}$), which form a non-negligible amount of stars and are therefore influenced by both internal and external baryonic effects. These are the subhaloes that are important for the too-big-to-fail problem, and the relative lack of these subhaloes in the baryonic simulations is key for solving the too-big-to-fail problem in the satellite populations of those hosts. Surprisingly, even without including the internal changes driven by feedback and bursty outflows, the embedded disc simulations capture these quantitative trends remarkably well: the accuracy of the embedded disc simulations is largely independent of subhalo mass at $r \lesssim 100$ kpc. This agreement suggests that subhalo survival near the centre of the host halo is dominated by gravitational interactions, such that these subhaloes are likely to suffer the same fate of disruption independent of their internal structure (on ∼500 pc scales). However, when including all subhaloes out to 300 kpc (see Appendix A), the disc simulations do overpredict the number of subhaloes with $V_{\rm max} \gtrsim 25\,\mathrm{km\,s^{-1}}$ by a factor of 3–5 relative to the baryonic simulations,

indicating that internal baryonic processes remain important in regulating the population of subhaloes at larger distances. These results generally agree with those of Brooks & Zolotov (2014), who found that tidal effects dominate for subhaloes that pass near the galactic disc.

Therefore, the tidal field from the central galaxy is partially responsible for eliminating some of the subhaloes that a too-big-to-fail analysis would identify as problematic 'massive failures' in a DMO simulation. As shown in Wetzel et al. (2016), `m12i` does not suffer from a too-big-to-fail problem when simulated with FIRE baryonic physics, indicating that a combination of internal feedback and tidal interactions resolves TBTF around that galaxy. The embedded disc potential alone reduces the number of subhaloes with $V_{\rm max} > 25\,{\rm km\,s^{-1}}$ within 300 kpc from 12 to 7, suggesting that the central galaxy is responsible for roughly half of the necessary changes *for this system*, with internal feedback driving lower inner densities in the surviving subhaloes and accounting for the remaining discrepancy. We draw similar conclusions from `m12f`, which hosts nine subhaloes with $V_{\rm max} > 25\,{\rm km\,s^{-1}}$ in the DMO run, but only 5 when simulated with an embedded disc, and identically zero when simulated with full physics. Of course, the exact relative contribution from internal feedback versus external tidal forces depends strongly on the individual histories of those large subhaloes, their spatial distribution within the host and, as we will show below, their orbital characteristics.

3.2 Destruction versus mass stripping?

In general, the tidal force from the central disc potential can either strip off a portion of the outer mass of a subhalo, shifting it to lower M and $V_{\rm max}$, or it can completely destroy the subhalo, through either tidal shocking (Gnedin, Hernquist & Ostriker 1999) or repeated stripping events, removing it from the population entirely. In order to distinguish between subhalo mass loss from total destruction, we measure subhaloes using $M_{\rm peak}$, defined as the largest virial mass that the main branch of each subhalo's merger tree reached. Thus, this quantity is preserved for a subhalo after infall and is not susceptible to mass loss, provided the subhalo survives to $z = 0$.

Fig. 4 shows the cumulative counts of resolved subhaloes within 100 kpc as a function of $M_{\rm peak}$. If the central galaxy typically strips subhaloes, but does not entirely destroy them, then the $M_{\rm peak}$ functions from the FIRE and disc simulations will agree with those of the DMO runs. Instead, at fixed $M_{\rm peak}$, the number of subhaloes is at least 2–3× larger in the DMO simulation, meaning that the central galaxy has destroyed at least 50–70 per cent of the substructure that currently resides within 100 kpc of the halo centre. As before, the embedded disc captures all but ∼10–20 per cent of this destruction, independent of $M_{\rm peak}$ except for the few largest subhaloes in `m12f`.

3.3 Which subhaloes are destroyed?

Thus far, we have examined subhaloes only as a function of their position at $z = 0$. However, we also can ask: out to what orbital pericentre distance are subhaloes significantly affected by the presence of the central disc? The left-hand panel of Fig. 5 shows the cumulative distribution of the pericentric distance, $d_{\rm peri}$, that subhaloes within 100 kpc that survive to $z = 0$ experienced, normalized to the total number of subhaloes within 100 kpc. We define $d_{\rm peri}$ as the smallest physical distance reached between the main branch of

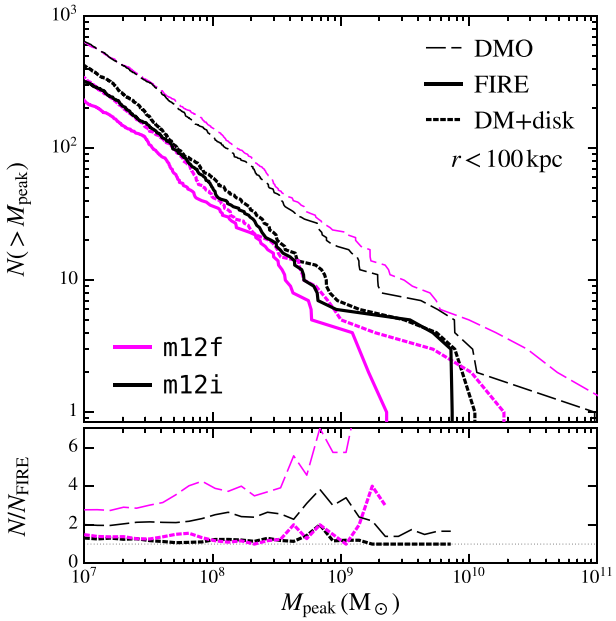

Figure 4. Cumulative number of subhaloes within <100 kpc at at $z = 0$, as in Fig. 3, but as a function of $M_{\rm peak}$, the largest virial mass ever attained by each subhalo (before any stripping). Though the agreement between the embedded disc and FIRE baryonic simulations are marginally worse than in Fig 2 or 3, which measured *instantaneous* $V_{\rm max}$ or bound mass M, the former still provide a better match to the FIRE simulations than the DMO predictions. Because $M_{\rm peak}$ is sensitive to destruction but is insensitive to (partial) mass stripping, this agreement indicates that, relative to the DMO simulations, the galactic disc primarily destroys subhaloes and removes them from the population – if subhaloes were stripped after infall, but survived until $z = 0$, then counts in the simulations with a central galaxy would agree nearly perfectly with those in the DMO simulations.

the host and that of a given subhalo.[5] The curves, which use the same colours and styles as previous Figures, are thus required to equal 1 at 100 kpc. The lower panel plots the ratio of the cumulative, non-normalized distributions, again relative to the FIRE baryonic simulations. The right-hand panel of Fig. 5, meanwhile, plots the (non-normalized) differential distribution of these same subhaloes.

Clearly, when a central galaxy is present, the orbit of a subhalo is important to its survival, and the differences in the distributions are stark: the median pericentric distances of the DMO samples are 20 kpc smaller than when the disc is included. Nearly every subhalo that reaches the central 10 kpc is destroyed by the central galaxy: only 2 (3) subhaloes that have passed within 10 kpc of the centre of `m12i` (`m12f`) survive to $z = 0$ in the baryonic simulations, whereas ∼100 such objects exist in the DMO runs. Similarly, 50 per cent of the surviving subhaloes have pericentric distances $\lesssim$20 kpc in the DMO simulation of `m12f`; that fraction drops to ∼5 per cent in both the baryonic and embedded disc simulations. The impact of the central galaxy is much weaker for subhaloes that have never passed within ∼30 kpc. This is in qualitative agreement with previous simulations by D'Onghia et al. (2010), who reached similar conclusions by inserting a disc potential into a halo extracted from a cosmological simulation.

[5] The positions of the two haloes are interpolated in a scale factor with a third-order spline to improve the time resolution, as in Fillingham et al. (2015).

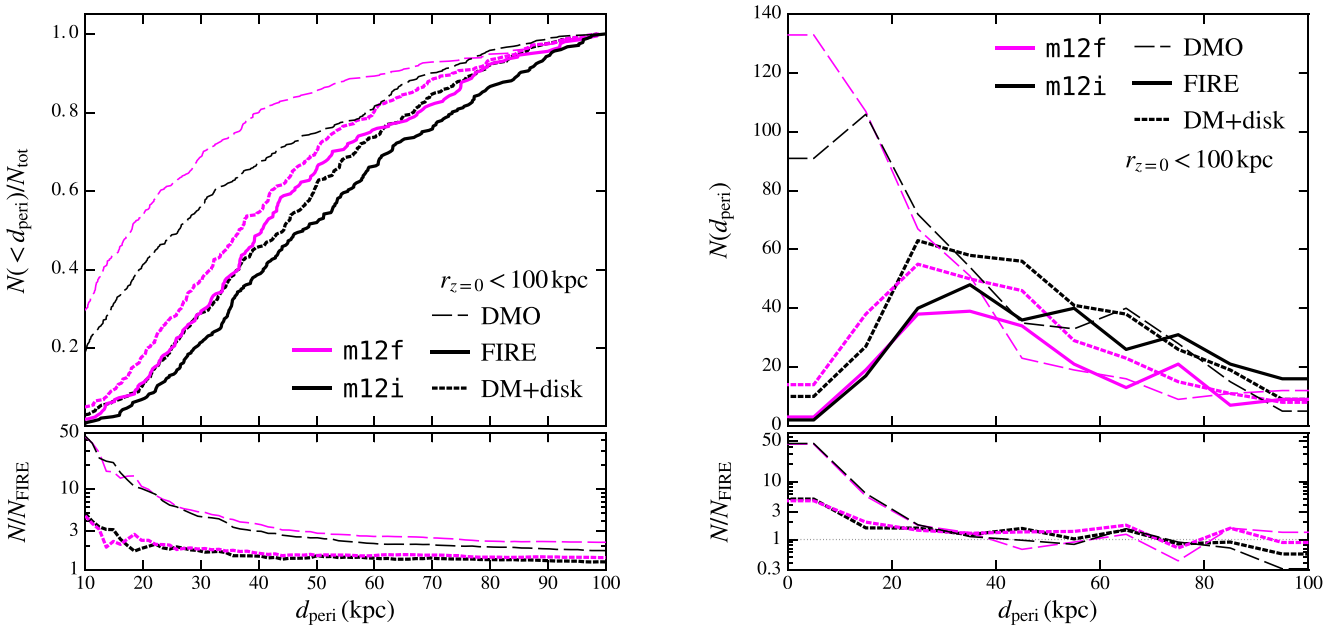

Figure 5. Cumulative (left) and differential (right) counts of subhaloes within 100 kpc at $z = 0$ as a function of their distance of closest approach to halo centre, $d_{\rm peri}$. The distributions in the left upper panel are normalized to the total number with $d_{\rm peri} < 100$ kpc, while the left lower panel indicates fractional differences in the *absolute* numbers; they are therefore not expected to equal 1 at $d_{\rm peri} = 100$ kpc. The distributions of pericentric distances in the DMO simulations far exceed those from the embedded disc or baryonic runs within $d_{\rm peri} \lesssim 30$ kpc, indicating that the central galaxy is responsible for subhalo destruction within that radius. DMO simulations overpredict the number of surviving subhaloes that passed within 10 kpc by a factor of ∼50 and within 20 kpc by ∼15×. The embedded disk simulations are accurate to within a factor of ≈2–4. The excess at $d_{\rm peri} \lesssim 20$ kpc in the disc runs is at least partially caused by not including the gaseous contribution: doubling the mass of the disc (Section 3.4) eliminates nearly all of the excess around `m12i`. The median pericentric distances experienced by surviving subhaloes in the simulations with a disc are ∼2 times larger than in the purely DMO simulations. The stark differences between the DMO and embedded disc simulations in these counts, which are insensitive to subhalo mass, suggest that the primary physical effect of the disc potential, particularly for those that come within ∼30 kpc, is to destroy subhaloes and remove them from the population, rather than to partially strip their mass.

The embedded disc simulations match the baryonic simulations well: the median pericentric distances are only ∼5 kpc smaller in the former, and the lower panels demonstrate that the distributions match better than a factor of 2 down to $d_{\rm peri} \approx 20$ kpc, though the embedded disc does overestimate the number of subhaloes with $d_{\rm peri} \sim 15$ kpc. The disc simulations remain an improvement over purely DMO simulations, however: the latter overpredict the number of surviving subhaloes that have passed within 10 kpc of a MW-like galaxy by a factor of ∼50. The remaining excess in the disc simulations is at least partially caused by the reduced central mass at early times due to our exclusion of gas from the disc model: doubling the mass of the disc at all times (Section 3.4) completely eliminates this discrepancy within 10 kpc, though such a change does overcorrect for the total mass in the FIRE simulations after $z \sim 1.5$.

The distributions plotted in Fig. 5 are largely independent of bound mass M: increasing the mass cut to only include subhaloes with $M > 3 \times 10^7\,{\rm M}_\odot$ yields nearly identical trends. Therefore, the sharp contrast between the DMO and embedded disc simulations further suggests that the primary role of the disc is to completely destroy subhaloes and remove them from the population, particularly for subhaloes that come near to the galaxy. In fact, the differences in the count of resolved subhaloes within 100 kpc of both hosts can be completely accounted for by the difference in the number of subhaloes with $d_{\rm peri} < 20$ kpc.

The distributions in Fig. 5 also inform our understanding of the differences between `m12i` and `m12f`. Specifically, the relative depletion in `m12f` is larger than that in `m12i`, likely because the pericentre distribution in the former is skewed to smaller radii, making its subhalo population more sensitive to the presence of a central galaxy.[6] This difference motivates the need to run many such simulations to explore the full range of subhalo orbital characteristics between hosts.

Fig. 2 showed that `m12i` and `m12f` baryonic simulations have *no* resolved subhaloes within 17–20 kpc of the central galaxy at $z = 0$. However, Fig. 5 shows that ≈20 subhaloes have orbited within this distance at some point, they simply are not located within this region by $z = 0$. Furthermore, Fig. 5 plots only pericentric distances of *surviving* subhaloes, and those that have been destroyed also could have induced dynamical effects in the inner halo, such as creating holes in stellar streams, prior to their destruction. That said, our results show that the total time-scales over which such subhaloes could act is significantly shorter. We leave the broader question of how streams form and evolve in fully cosmological simulations that include a central galaxy for later work.

Fig. 5 clearly shows that ≳90 per cent of subhaloes that pass within 10–20 kpc of the central galaxy are destroyed. This dependence on pericentre implies that the velocity distribution of *surviving* subhaloes should be significantly biased relative to DMO

[6] While `m12i` and `m12f` have a similar total mass within a 2 Mpc sphere, `m12f` is within a more filamentary environment, which may explain why its satellites have more radial orbits.

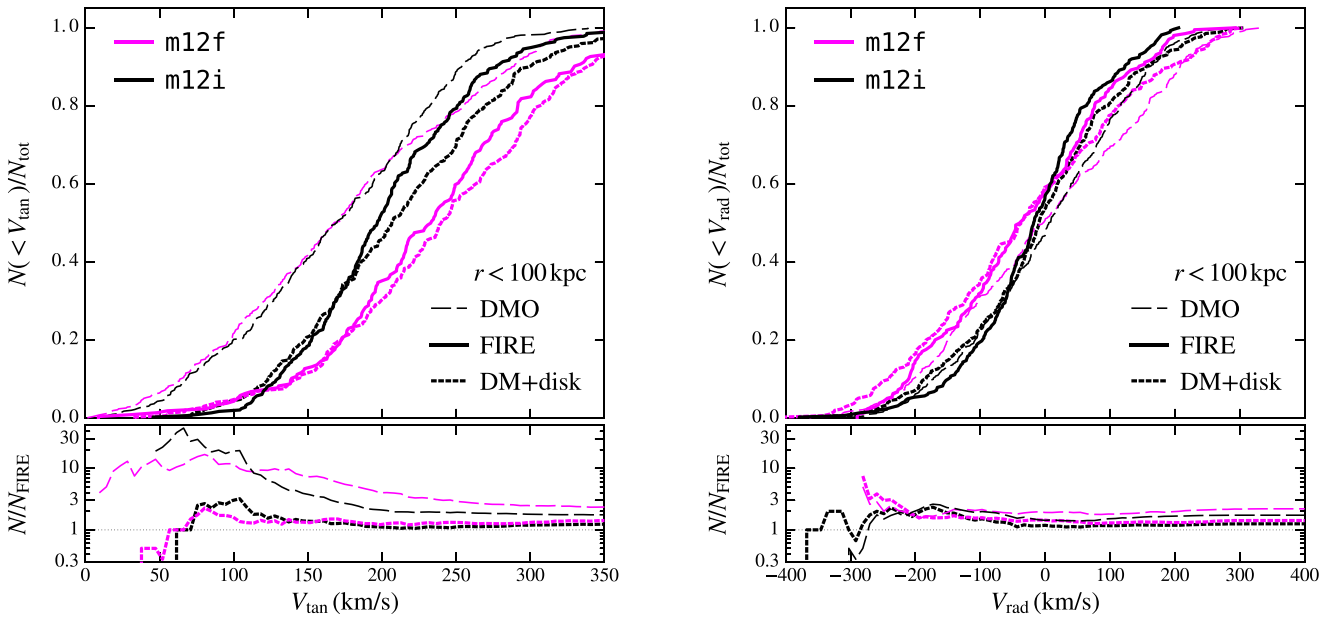

Figure 6. Cumulative distribution of tangential (left) and radial (right) velocities of resolved subhaloes within 100 kpc of the centre of `m12i` (black lines) and `m12f` (magenta lines) at $z = 0$, normalized to the total number within 100 kpc. Consistent with the baryonic simulations, the embedded disc preferentially destroys subhaloes that are on radial orbits (low $V_{\rm tan}$) that pass close to the disc. Similarly, subhaloes with high radial velocities ($V_{\rm rad} \gtrsim 75\,{\rm km\,s^{-1}}$) are slightly suppressed in the baryonic and embedded disc simulations, but the difference is far less pronounced than in $V_{\rm tan}$. As in Fig. 5, the lower panels show the fractional difference in the absolute (non-normalized) cumulative distribution.

simulations, such that systems on radial, plunging orbits with low specific angular momentum should be preferentially destroyed.

The left-hand panel of Fig. 6 shows the cumulative distribution of the tangential velocities, $V_{\rm tan}$, of subhaloes within 100 kpc, normalized to the total number within 100 kpc, demonstrating the strength of this effect. While subhaloes in the DMO simulation have a mean $V_{\rm tan}$ of $\sim$150 km s^{-1}, the presence of a central galaxy increases it to $\sim$200–250 km s^{-1}. The lower panel, which again plots the ratio in the absolute distributions, demonstrates that the DMO simulations overpredict the number of subhaloes within 100 kpc with $V_{\rm tan} < 100\,{\rm km\,s^{-1}}$ by a factor of 10. The embedded disc simulations, however, agree to within a factor of 2–3 at all $V_{\rm tan}$. While the suppression of subhaloes with low $V_{\rm tan}$ in runs with a central galaxy is primarily caused by the destruction of those systems, the deeper potential well in the central regions also leads to an increase in the velocities of surviving systems near the galaxy.

We similarly examine the distributions of subhalo radial velocities in the right-hand panel of Fig. 6. However, in contrast to the tangential distributions, we find that they agree across all simulations to within $\sim$50 per cent at most $V_{\rm rad}$. We do find that the relative fraction of subhaloes with large, positive radial velocities ($V_{\rm rad} \gtrsim 75\,{\rm km\,s^{-1}}$) is slightly suppressed in the simulations with a central galaxy relative to the DMO simulations, as expected if subhaloes that have passed close to the halo centre and would be moving away from the host are preferentially destroyed. However, overall these results indicate that *a subhalo's likelihood of being destroyed by the central galaxy does not depend significantly on its radial velocity*. As a result, the primary effect of the central galaxy is on the resultant distribution of tangential, and not radial, velocities of the surviving subhalo population. There is a slight trend wherein the pure DMO simulations underpredict the fraction of high $|V_{\rm rad}|$ subhaloes (i.e. overpredict the fraction of systems with $V_{\rm rad} \sim 0\,{\rm km\,s^{-1}}$), consistent with an overall increase in subhalo velocities in the presence of a galaxy due to the added mass at the centre of the host.

This tangential velocity bias may have direct consequences on the expected perturbations induced in the cold stellar streams that are suggested as best able to constrain dark subhalo counts in the MW, which stretch along the plane of the sky (e.g. Newberg & Carlin 2016). Specifically, if both the observed streams and the subhalo population are tangentially biased, one would expect more 'glancing' blows, wherein subhaloes are either corotating or counterrotating relative to the orbit of the stream, and fewer perpendicular interactions, where the subhalo punches directly through a cold stream, relative to what is expected for an isotropic population of subhaloes (the standard assumption in most work on stream–subhalo interactions; e.g. Yoon et al. 2011; Carlberg 2012; Erkal et al. 2016). Counterrotating interactions will have a small impact on streams due to their relatively short interaction times, but a larger fraction of the encounters may by corotating than otherwise expected. These occur over long enough time-scales that the impulse approximation typically used to estimate changes in the stellar velocities (e.g. Sanders et al. 2016) may break down. We defer a full analysis of the degree to which this effect is observable to future work.

Similarly, the preferential destruction of subhaloes on highly radial orbits has important implications for the structure of the stellar halo, particularly close to the MW. Specifically, the majority of the destroyed satellites that make up the stellar halo (Bullock, Kravtsov & Weinberg 2001; Bullock & Johnston 2005; Bell et al. 2008) were likely on plunging, highly radial orbits, such that their resultant stellar streams are likely to be radially extended and reach to greater radii. Therefore, streams from destroyed satellites may prove useful for detecting clear, coherent gaps from the surviving dark subhaloes, which are largely on tangential orbits that are perpendicular to the expected orientations of the streams from destroyed satellites.

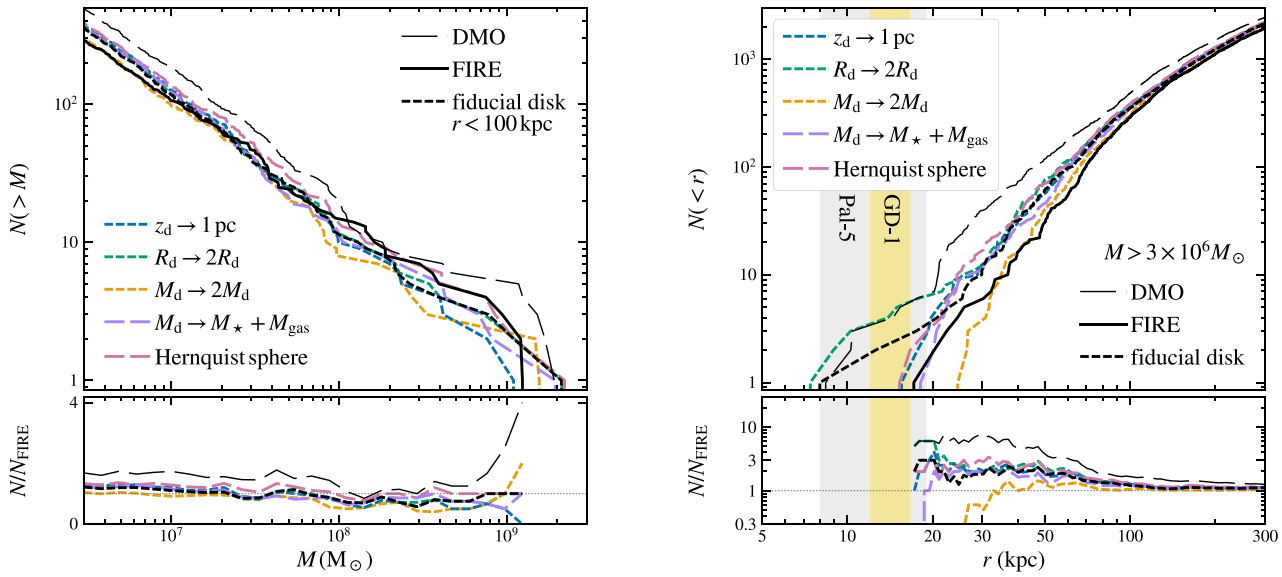

Figure 7. How varying the properties of the embedded disc in `m12i` affects the subhalo population at $z = 0$. Black lines are identical to Fig. 2. The coloured dashed lines show embedded disc models with factors of 2 changes the scale radius, R_d and the total mass M_d, with a 1 pc thin disc, and with a total mass M_d equal to the stellar mass plus the gas mass within the galaxy, while the dashed light red line shows the results of adding the potential from a Hernquist sphere of identical total mass to the simulation; details are provided in the text. Left: Cumulative counts of subhaloes above a given bound mass, M, within 100 kpc of the centre at $z = 0$. Right: Cumulative counts of resolved subhaloes within a given radius, r. The results are largely independent of the radius or thickness of the disc, indicating that the shape and orientation of the potential are sub-dominant factors – the spherically symmetric Hernquist (1990) potential destroys nearly as many subhaloes as the disc, though the excess in this run relative to the fiducial disc suggests that disc shocking is responsible for some of the destruction. However, doubling the mass of the disc (orange dashed line) has a larger effect and causes significantly more subhalo destruction, leading to somewhat better agreement with the FIRE baryonic simulation, particularly within ∼50 kpc. This improved agreement is likely because we originally match to only the stellar component of the central disc; doubling the disc mass roughly accounts for non-negligible gaseous contribution, particularly at $z \gtrsim 1$. Overall, we emphasize that even imperfect fits to the disc provide a more accurate description of the subhalo population predicted by the fully baryonic simulation at nearly all masses and radii than a purely DMO realization.

3.4 Varying the disc parameters

In order to explore the dependence on the specific disc potential that we add to the DM simulations, we additionally simulate `m12i` with modified disc parameters. Specifically, we hold two of the three disc parameters, $R_d(z)$, $z_d(z)$ and $M_d(z)$ (see equation 1) at their fiducial values, while varying the third. We investigate: $R_d(z) \rightarrow 2R_d(z)$, spreading the same amount of mass over a larger surface area; $z_d \rightarrow 1$ pc at all times, forcing a nearly infinitesimally thin disc; and $M_d(z) \rightarrow 2M_d(z)$, making the disc more massive. We also test the dynamical importance of the gas in the galaxy by holding R_d and z_d fixed at their fiducial values, but setting M_d equal to the fiducial (stellar) mass plus the mass in gas within r_{90} (i.e. $M_d \rightarrow M_\star + M_{gas}$). In order to further test the importance of the shape and orientation of the galactic potential, we also simulate `m12i` with a Hernquist (1990) sphere, rather than the Miyamoto–Nagai disc potential.

Fig. 7 shows the bound mass functions (left) and cumulative radial distributions (right) of these simulations, along with the three versions of `m12i` presented previously. The solid, dashed and dotted black lines are identical to those in the left-hand panels of Fig. 2, while the green, blue and orange lines indicate the results of the simulations with $2R_d$, $z_d = 1$ pc and $2M_d$, respectively. The lavender lines plot counts obtained by additionally including the gas in the mass in the disc, and the light red dashed line plots subhalo counts with a Hernquist potential of identical mass and radial extent, quantified by r_{90}.

In summary, subhalo depletion most directly correlates with the mass of the central disc. The simulation with the $2M_d$ disc results in fewer subhaloes, especially at $r \lesssim 70$ kpc. The $2R_d$ disc yields slightly more subhaloes at small r, while the dependence on z_d is weak, with the $z_d = 1$ pc disc predicting slightly fewer subhaloes than the fiducial disc. The shape, and consequently the orientation, of the potential appears to be of secondary importance, with the $z_d = 1$ pc disc and the Hernquist sphere both yielding very similar results to the fiducial disc. However, the slight excess in the simulation with a Hernquist potential, relative to the fiducial disc, suggests that some subhaloes are destroyed by disc shocking that would otherwise survive the enhanced tidal forces (see also D'Onghia et al. 2010). Therefore, small gains may be achieved by matching the orientation of the real galaxy, but we emphasize again that even a disc with an imperfect, fixed orientation yields subhalo populations with distributions that typically agree to within ∼25 per cent, without the additional complexity of determining the correct orientation.

Interestingly, at most masses and radii, the $2M_d$ disc in fact yields a slightly better match to the FIRE baryonic simulation than the fiducial disc simulation.[7] As noted in Section 2.1, we match the mass of the fiducial disc to the stellar disc that forms in the baryonic simulation, but this neglects the (complex) contribution from (fluctuating) gas in/near the disc. Therefore, we *may* posit that this improved match is a consequence of more accurately matching the *total* baryonic mass at the centre of the halo at early times, when the disc is dominated by gas ($z \gtrsim 1$).

[7] The $2M_d$ simulation also provides a better match to the d_{peri}, V_{tan} and V_{rad} distributions of the FIRE baryonic simulations than the fiducial disc.

However, the simulation with $M_{\rm d} \rightarrow M_\star + M_{\rm gas}$ differs only slightly from the results of the fiducial disc: adding the gas to the disc mass yields marginally fewer subhaloes at fixed mass and radius. Because the differences in the disc mass between this run and the fiducial run occur primarily at early times,[8] the close agreement between the two runs suggests that the mass at early times is relatively unimportant, likely because the majority of subhaloes fall into the MW-size host halo after $z = 1$ (e.g. Wetzel, Deason & Garrison-Kimmel 2015a). The lingering discrepancy between the $M_\star + M_{\rm gas}$ run and the fully hydrodynamical simulation further indicates that the gas does have important, if second-order, dynamical effects on subhaloes due to a combination of internal feedback, ram pressure and viscous stripping in the hot halo, and interactions with inflows and outflows.

Overall, we emphasize that factors of ∼2 changes to the parameters of the embedded discs have a relatively modest effect on the subhalo population at $z = 0$, as compared with the much stronger difference from *not* using an embedded disc. Moreover, our experiments with the shape of the potential show that the detailed geometry and orientation of the disc (difficult to predict in non-fully baryonic simulations) are of small, secondary importance: what matters (to leading order) is a central potential of the correct baryonic mass and radial size. Thus, even if the exact galaxy that *would* form in a given halo is not completely constrained, one still can improve upon the predictions of DMO simulation by inserting a central galaxy with parameters drawn from empirical scaling relations.

3.5 Comparison with Sawala et al. (2017)

Recently, Sawala et al. (2017, hereafter S17) demonstrated that the subhalo populations of four of the hosts in the APOSTLE project (Fattahi et al. 2016; Sawala et al. 2016), which simulates MW/M31-like pairs of haloes using the EAGLE prescriptions for star formation and feedback (Schaye et al. 2015), are suppressed relative to their DMO counterparts. Here we explicitly compare their results to the differences that arise between the FIRE simulations and their DMO analogues.

Fig. 1 of S17 indicates that at the lowest masses resolved by the APOSTLE simulations, the DMO counterparts overpredict subhalo counts within 300 kpc by a factor of ∼1.3. While the DMO analogues of the Latte simulations overpredict subhalo counts within 100 kpc by a factor of ∼2–3 (Fig. 2), the ratio of $N(>M)_{\rm DMO}/N(>M)_{\rm FIRE}$ within 300 kpc is roughly 1.2–1.5 (Fig. A2), in close agreement with the results of S17. At smaller radii, however, fig. 3 of S17 suggests that the DMO simulations typically overpredict counts within 50 kpc by a factor of ∼1.75–2, while our results (Fig. A1) suggest that DMO simulations overpredict counts within 50 kpc by a factor of 3–4. Accordingly, we predict a larger discrepancy (between DMO and hydrodynamical simulations) in the radial distributions at small distances: subhalo densities at $r \sim 30$ kpc are a factor of ∼4 times higher in the DMO analogues than in the FIRE simulations, while fig. 4 of S17 indicates that their DMO analogues only predict a factor of ∼1.6 discrepancy at the same radius.

Therefore, while our general conclusions regarding depleted radial distributions agree well, results from the FIRE simulations suggest that the discrepancy grows larger at small radius ($r < 100$ kpc), but the results of S17 indicate a roughly constant offset within ∼50 kpc. While this disagreement is second-order, it may be due to differences in the central masses of the galaxies that form in the two sets of simulations. Per fig. 7 of Fattahi et al. (2016), the APOSTLE discs tend to lie slightly below expectations from abundance matching analyses. Both `m12i` and `m12f`, however, fall slightly above those same relationships (Hopkins et al. 2017). As evidenced by the parameter survey presented in Section 3.4, increasing the mass density at the centre of host destroys more satellites at small radii without strongly altering results at $r \gtrsim 100$ kpc.

We caution, however, that the results in S17 are based on the subhalo populations of only four hosts, and that our results include only two hosts. Because some degree of halo-to-halo scatter is expected, it is not clear that our results should agree exactly with those of S17. It is encouraging, therefore, that all six hosts demonstrate a similar trend: a clear reduction in subhalo populations, with the largest differences occuring within ∼50–100 kpc and with subhaloes on radial orbits (low tangential velocities) preferentially depleted (fig. 8 of S17).

4 IMPLICATIONS

DMO simulations have been used extensively to interpret data and to make predictions for subhalo observables. Here we briefly discuss several such investigations that are likely affected by our results and speculate how the effects of a central galaxy potential in more massive haloes could affect the broader use of DM simulations to interpret data.

As discussed in Sections 1 and 3, the significant depletion that we see in our baryonic and embedded disc simulations at small radii has important implications for ongoing searches for substructure in the MW halo. Perhaps the most promising method involves looking for gaps and other anomalies in the stellar streams of Palomar-5 and GD-1. Both of these streams exist within 20 kpc of the Galaxy, therefore they sit within the region that is most severely depleted (see Fig. 2). Our results imply that there may be no dark substructures in such a region today to affect these streams, and that even if they orbited in this region in the past, their lifetime is much shorter than predicted from DMO simulations. However, further work is needed to sample full subhalo evolutionary histories, and as we discuss in the next section, a more focused effort on simulating tuned MW analogues (set to the mass of the MW galaxy, rather than being matched to a comparison hydrodynamical simulation) with a statistical sample of initial conditions will be required to determine the range of subhalo counts that we expect around our Galaxy within this region.

More generally, any analyses that depend strongly on the subhalo mass function, the radial distribution or the velocity distribution, particularly near the centre of the host, will be severely impacted by the presence of a central galaxy. One example is the expected completeness corrections to the faint-end of the MW stellar mass function (Tollerud et al. 2008; Hargis, Willman & Peter 2014). This depends non-trivially on the radial distribution of subhaloes, because the correction is based on how many more subhaloes we expect to exist within some large volume (e.g. $r \leq 400$ kpc) given an observed number within a smaller (e.g. $r \leq 100$ kpc), observationally complete volume. The enhanced central depletion in our simulations suggests that there are fractionally even more satellites waiting to be discovered at large radii, given the number that we currently observe within the completeness limits of SDSS, DES or Pan-STARRS. As pointed out by Ahmed, Brooks & Christensen

[8] While adding the gas mass drastically increases the mass of the disc at early times (by a factor of ∼10 at $z = 3$), the contribution after $z = 1$ is less than a factor of 2, and the total mass is within ∼15 per cent of the fiducial (stellar) mass by $z = 0.5$.

(2017), who also found that subhalo populations are more radially extended in baryonic simulations than in DMO, depleting the central region of substructure has the additional effect of increasing the statistical significance of any potential 'planes of satellites.'

The missing satellites problem is clearly reduced in severity by the destruction of subhaloes with $M \sim 10^9$–$10^{10}\,\mathrm{M}_\odot$. Similarly, the tension in comparing the number of dwarf galaxies containing old stars around the MW with expectations from the observed steep luminosity functions during the reionization era, as discussed by Boylan-Kolchin, Bullock & Garrison-Kimmel (2014), will be reduced; many of those ancient stars instead would be dispersed into the stellar halo via the enhanced disruption brought on by the central disc. Similarly, the constraints on stellar mass functions at $z \sim 5$ based on MW galaxy counts presented in Graus et al. (2016) will be modified.

Limits on warm DM models (e.g. Horiuchi et al. 2014, 2016) associated with requiring enough subhaloes to host the known satellites will become even tighter. Predictions for the substructure boost for DM annihilation signals in the Galactic centre (Kuhlen, Diemand & Madau 2008; Bovy 2009) will decrease. However, subhaloes would still be expected to contribute to a boost at larger radii, which could be important for indirect detection searches around the M31 halo or in the all-sky background from the MW halo itself.

The reduction in subhalo counts also modifies the results of using counts of satellite galaxies in the Local Group to constrain the $M_\star - M_{\rm halo}$ relation at low masses (e.g. Brook et al. 2014; Garrison-Kimmel et al. 2014a, 2017). Specifically, matching to fewer DM haloes, as implied by our results, requires a flatter log-slope, which also shifts the relation closer towards one that alleviates the 'too-big-to-fail' problem (Boylan-Kolchin et al. 2011, 2012; Garrison-Kimmel et al. 2014b; Papastergis et al. 2015, and see also Jethwa et al. 2016). The effect of enhanced disruption from a central disc in alleviating the too-big-to-fail problem was first emphasized by Brooks & Zolotov (2014).

The preferential destruction of subhaloes on plunging orbits also has consequences for analyses that utilize the velocity distributions of subhaloes in DMO simulations. For example, the number of 'backsplash galaxies' (galaxies beyond the virial radius of a more massive host that orbited within the virial radius in the past; e.g. Teyssier, Johnston & Kuhlen 2012; Wetzel et al. 2014; Garrison-Kimmel et al. 2014a) that have passed close to the central galaxy should be drastically reduced, though the number that have had only glancing encounters with the host halo will be largely unaltered. Similarly, the works of Fillingham et al. (2015) and Wetzel, Tollerud & Weisz (2015b) explored the time-scales over which the satellite galaxies of the MW and M31 had their star formation quenched after infall using subhalo catalogs taken from the ELVIS simulations. While they found that the environmental quenching time-scales of satellite dwarf galaxies are short ($\lesssim$2 Gyr; much shorter than for more massive satellites), our results imply *even shorter* quenching time-scales, because many of the subhaloes that fell in at early times have preferentially smaller pericentres (Wetzel et al. 2015a) and therefore should be destroyed by the central galaxy. Because satellites with low tangential velocities also are destroyed with high efficiency; however, the constraints on ram-pressure stripping from Fillingham et al. (2016) may become less stringent. Similarly, the recent discrepancy pointed out by Cautun & Frenk (2017), wherein the MW satellites are on more tangentially biased orbits than expected from ΛCDM, is alleviated by the destruction of these low $V_{\rm tan}$ subhaloes.

While our analysis focused on MW-size haloes, substructure depletion caused by a central galaxy is likely important around larger ($M_{\rm halo} \sim 10^{13}\,\mathrm{M}_\odot$) galaxies as well. This is particularly relevant for searches for dark subhaloes via lensing anomalies (e.g. Vegetti et al. 2010; MacLeod et al. 2013; Nierenberg et al. 2014; Hezaveh et al. 2016). However, the strength of the impact of these more massive galaxies on their subhaloes is unclear. The MW represents the mass at which the ratio of central galaxy stellar mass to host halo mass is highest (Leauthaud et al. 2012; Behroozi, Wechsler & Conroy 2013b; Moster, Naab & White 2013), so this is the mass scale at which the central galaxy most strongly affects the halo potential. Thus, the effect in larger hosts may be weaker. Furthermore, more massive haloes generally assemble at later times (with satellites falling in later), suggesting that subhalo destruction may be further suppressed relative to our findings here.

In fact, Fiacconi et al. (2016) recently presented two baryonic simulations of galaxies in this mass regime, and found that baryonic contraction actually increases the number of massive subhaloes near the centre of the host relative to DMO simulations. However, Graus et al. (in preparation) perform a similar analysis using the Illustris and Illustris Dark simulations (Vogelsberger et al. 2014a,b) and find the opposite effect: the baryonic simulations have fewer subhaloes at $\sim 10^8\,\mathrm{M}_\odot$ around lens hosts, with the largest deficit near the central regions. Despali & Vegetti (2017) similarly compared the DMO and baryonic versions of the Illustris and EAGLE (Schaye et al. 2015) simulations, and demonstrated that subhalo counts around hosts of mass $10^{12.5}$–$10^{14}\,\mathrm{M}_\odot$ are suppressed by ∼30 per cent at subhalo masses $10^9\,\mathrm{M}_\odot$ in the baryonic simulations, with the largest suppression near the centre of the hosts (see also Chua et al. 2016, who reached similar conclusions using the Illustris simulations). The impact on the lowest-mass subhaloes, however, remains largely unexplored due to the difficulty of simulating galaxies of this mass at high resolution with baryonic physics.

Finally, if a similar degree of substructure depletion occurs for roughly LMC to MW-size subhaloes ($M_{\rm halo} \sim 10^{11}$–$10^{12}\,\mathrm{M}_\odot$) around massive hosts ($M_{\rm halo} \gtrsim 10^{14}\,\mathrm{M}_\odot$), it could have important implications for the use of DMO simulations to interpret small-scale ('one-halo') clustering statistics through subhalo abundance matching (e.g. Conroy, Wechsler & Kravtsov 2006; Reddick et al. 2013), as compared with studies that examined these trends for subhalo disruption without modelling a central galaxy (e.g. Wetzel & White 2010). Specifically, if the subhaloes that are massive enough to host bright galaxies ($M_\star \gtrsim 10^{10}\,\mathrm{M}_\odot$) are preferentially depleted in galaxy groups owing to the potential of the brightest cluster galaxy, then abundance matching analyses would tend to assign too little stellar mass to subhaloes of a given M to avoid overproducing those galaxies. If this effect is important in groups and clusters, then it may also influence the use of similar approaches to understand trends between galaxy colour and age with subhalo accretion times (e.g. Mahajan, Mamon & Raychaudhury 2011; Wetzel et al. 2013; Hirschmann et al. 2014; Oman & Hudson 2016). However, the increased concentrations of MW-mass subhaloes in baryonic simulations may also make these systems more resistant to stripping (e.g. Chua et al. 2016), such that even if there are fewer satellites overall, a greater proportion of those remaining would have $M_{\rm halo} \sim 10^{12}\,\mathrm{M}_\odot$ than DMO simulations would predict.

5 CONCLUSIONS

The interplay between DM and baryons, and the subsequent importance of baryons in correctly predicting the properties of DM haloes with cosmological simulations, has a rich history in this field (e.g. di Cintio et al. 2011; Governato et al. 2012; Pontzen &

Governato 2012; Zolotov et al. 2012; Arraki et al. 2014; Brooks & Zolotov 2014; Sawala et al. 2015; Di Cintio et al. 2014; Chan et al. 2015; Oñorbe et al. 2015; Cui et al. 2016; Sawala et al. 2016; Wetzel et al. 2016). In this paper, we explored the role of baryons in affecting the low-mass subhaloes of interest for observational searches for dark subhaloes: DM mass $M > 3 \times 10^6\,\mathrm{M}_\odot$; $V_{\rm max} > 5\ \mathrm{km\ s^{-1}}$.

Our exploration relied on two MW-mass DM haloes from the Latte simulation suite (Wetzel et al. 2016), each simulated (1) with full baryonic physics from the FIRE project, (2) with DM only, and (3) with DM plus an embedded disc potential for the central galaxy that evolves to match the stellar disc in the corresponding baryonic simulation. As shown in Fig. 2, relative to the DMO simulations, subhalo counts in the baryonic simulations are lower by a factor of ∼5 within 25 kpc of the halo centre. Both of the baryonic simulations are *completely* devoid of substructure within 15 kpc at $z = 0$, though ∼20 subhaloes with pericentric distances <20 kpc survive to the present day. Subhalo depletion becomes less important with increasing radius: within ∼300 kpc (roughly the halo virial radius), subhalo counts in the baryonic simulations are lower by only ∼15–30 per cent compared to the DMO simulations. This depletion is driven by the preferential destruction of subhaloes on radial orbits that get to $d_{\rm peri} \lesssim 30$ kpc from the halo centre. This in turn biases the orbital velocities of *surviving* subhaloes at $z = 0$ to be more tangential in simulations that have central galaxies than they are in DMO simulations.

Importantly, the simulations with embedded disc potentials reproduce at least ∼75 per cent of the depletion evident in the mass functions and radial distributions. This good agreement is important for two reasons. First, because we carefully matched the evolving disc potential to the stellar disc in the baryonic simulations, this comparison provides a clear physical explanation for the origin of subhalo depletion in the baryonic simulations: the bulk of the subhalo depletion arises simply from the tidal field of the central galaxy itself. These results also imply that the majority of subhalo depletion is *independent* of the exact model of feedback or star formation, because our embedded disc simulations include none of these. However, we emphasize that we matched the evolving disc potential to the *stellar mass* in the baryonic simulations; this therefore provides a conservative underestimate of the total baryonic mass of the central galaxy, especially at early times when the simulated galaxies were gas rich. As Fig. 7 showed, though, adding the approximate gas mass to the disc yields only marginally better agreement between the embedded disc and baryonic simulations. Therefore, a small fraction of the substructure depletion is *not* due to interactions with the central galaxy, and cannot be captured with this technique.

Second, given its significantly improved accuracy as compared with DMO simulations, our method of embedding a central disc potential provides an inexpensive way to significantly improve the accuracy of DMO simulations. The population statistics of surviving subhaloes in the embedded disc simulations display much better agreement with those in the FIRE baryonic simulations in every statistic that we have checked, including infall times, pericentric distances, radial velocities, total orbital velocities, radial profiles and counts as a function of mass at $z = 0$ or at infall. We also find that the disc simulations yield more accurate counts around the hosts at higher redshift, though the differences are less dramatic than at $z = 0$. Thus, one can vastly improve upon predictions from purely DMO simulations, at nearly the same CPU cost, by simply including a central galactic potential.

Moreover, as Fig. 7 showed, subhalo depletion is largely insensitive to the central disc thickness, and it depends only mildly on disc radius and the detailed shape of the potential. The most important parameter is simply the central galaxy mass. Thus, one can (to reasonable approximation) adopt a simple, spherically symmetric analytic potential with parameters taken from observations (e.g. abundance-matching) or large-volume simulations.

The differences that we see between simulations with and without central galaxies are particularly important for dark substructure searches that rely on cold stellar streams within 20 kpc of the Galaxy. However, it is difficult to estimate the expected halo-to-halo variance based on just two haloes. As shown in Fig. 5, the intrinsic pericentre distribution for a given subhalo population can vary considerably, which likely affects subhalo disruption considerably. A larger suite of hosts simulated with embedded discs that match the MW is required to make more concrete statistical statements (Kelley et al., in preparation).

We demonstrated that baryonic effects are crucially important for interpreting ongoing substructure searches. Galaxies exist within the centres of haloes and are dynamically important within the vicinity of discs like the MW. Our method of embedding galactic potentials in cosmological zoom-in simulations provides an avenue to producing more accurate substructure predictions, relative to baryonic simulations, without the millions of CPU hours required by those simulations. These embedded galaxies therefore hold the promise of improved predictions for the statistical properties of subhalo populations, which are necessary to fully interpret the results of many upcoming observations, including those aimed at detecting tiny, dark subhaloes.

ACKNOWLEDGEMENTS

The authors thank Jo Bovy, Mia Bovill and Brandon Bozek for valuable discussions and the anonymous referee for several suggestions that have improved the manuscript. The authors also thank Erik Tollerud for providing software used to create visualizations and Alexander Knebe, Peter Behroozi, and Oliver Hahn, respectively, for making `AHF`, `consistent-trees`, and `MUSIC` publicly available.

Support for SGK was provided by NASA through Einstein Postdoctoral Fellowship grant number PF5-160136 awarded by the Chandra X-ray Center, which is operated by the Smithsonian Astrophysical Observatory for NASA under contract NAS8-03060. AW was supported by a Caltech-Carnegie Fellowship, in part through the Moore Center for Theoretical Cosmology and Physics at Caltech, and by NASA through grant HST-GO-14734 from STScI. JSB and TK were supported by NSF grant AST-1518291 and by NASA through HST theory grants (programs AR-13921, AR-13888, and AR-14282.001) awarded by the Space Telescope Science Institute (STScI), which is operated by the Association of Universities for Research in Astronomy (AURA), Inc., under NASA contract NAS5-26555. Support for PFH was provided by an Alfred P. Sloan Research Fellowship, NASA ATP Grant NNX14AH35G, and NSF Collaborative Research Grant #1411920 and CAREER grant #1455342. MBK acknowledges support from the National Science Foundation (grant AST-1517226) and from NASA through HST theory grants (programs AR-12836, AR-13888, AR-13896 and AR-14282) awarded by STScI. CAFG was supported by NSF through grants AST-1412836 and AST-1517491, and by NASA through grant NNX15AB22G. DK acknowledges support from NSF grant AST-1412153 and the Cottrell Scholar Award from the Research Corporation for Science Advancement. EQ was supported by NASA ATP grant 12-APT12-0183, a Simons Investigator award from the Simons Foundation, and the David and Lucile Packard

Foundation. Support for ASG was provided by NSF grant AST-1009973.

Numerical calculations were run on the Caltech compute cluster 'Zwicky' (NSF MRI award #PHY-0960291) and allocation TG-AST130039 granted by the Extreme Science and Engineering Discovery Environment (XSEDE) supported by the NSF. Resources supporting this work were also provided by the NASA High-End Computing (HEC) Program through the NASA Advanced Supercomputing (NAS) Division at Ames Research Center. This work also made use of ASTROPY, a community-developed core Python package for Astronomy (Astropy Collaboration et al. 2013), MATPLOTLIB (Hunter 2007), NUMPY (van der Walt, Colbert & Varoquaux 2011), SCIPY (Jones et al. 2001), IPYTHON (Perez & Granger 2007), MAYAVI (Ramachandran & Varoquaux 2011), and NASA's Astrophysics Data System.

REFERENCES

Ahmed S. H., Brooks A. M., Christensen C. R., 2017, MNRAS, 466, 3119
Amorisco N. C., Zavala J., de Boer T. J. L., 2014, ApJ, 782, L39
Amorisco N. C., Gómez F. A., Vegetti S., White S. D. M., 2016, MNRAS, 463, L17
Arraki K. S., Klypin A., More S., Trujillo-Gomez S., 2014, MNRAS, 438, 1466
Astropy Collaboration; Robitaille T. P. et al., 2013, A&A, 558, A33
Behroozi P. S., Wechsler R. H., Wu H.-Y., Busha M. T., Klypin A. A., Primack J. R., 2013a, ApJ, 763, 18
Behroozi P. S., Wechsler R. H., Conroy C., 2013b, ApJ, 770, 57
Bell E. F. et al., 2008, ApJ, 680, 295
Berezinsky V., Dokuchaev V., Eroshenko Y., 2006, Phys. Rev. D, 73, 063504
Bland-Hawthorn J., Gerhard O., 2016, ARA&A, 54, 529
Bode P., Ostriker J. P., Turok N., 2001, ApJ, 556, 93
Bose S., Hellwing W. A., Frenk C. S., Jenkins A., Lovell M. R., Helly J. C., Li B., 2016, MNRAS, 455, 318
Bovy J., 2009, Phys. Rev. D, 79, 083539
Bovy J., Erkal D., Sanders J. L., 2017, MNRAS, 466, 628
Boylan-Kolchin M., Bullock J. S., Kaplinghat M., 2011, MNRAS, 415, L40
Boylan-Kolchin M., Bullock J. S., Kaplinghat M., 2012, MNRAS, 422, 1203
Boylan-Kolchin M., Bullock J. S., Garrison-Kimmel S., 2014, MNRAS, 443, L44
Bozek B., Boylan-Kolchin M., Horiuchi S., Garrison-Kimmel S., Abazajian K., Bullock J. S., 2016, MNRAS, 459, 1489
Brook C. B., Di Cintio A., Knebe A., Gottlöber S., Hoffman Y., Yepes G., Garrison-Kimmel S., 2014, ApJ, 784, L14
Brooks A. M., Zolotov A., 2014, ApJ, 786, 87
Bryan G. L., Norman M. L., 1998, ApJ, 495, 80
Bullock J. S., Johnston K. V., 2005, ApJ, 635, 931
Bullock J. S., Kravtsov A. V., Weinberg D. H., 2000, ApJ, 539, 517
Bullock J. S., Kravtsov A. V., Weinberg D. H., 2001, ApJ, 548, 33
Carlberg R. G., 2012, ApJ, 748, 20
Carlberg R. G., 2013, ApJ, 775, 90
Carlberg R. G., Grillmair C. J., Hetherington N., 2012, ApJ, 760, 75
Catinella B. et al., 2010, MNRAS, 403, 683
Catinella B. et al., 2012, A&A, 544, A65
Catinella B. et al., 2013, MNRAS, 436, 34
Cautun M., Frenk C. S., 2017, MNRAS, 468, L41
Chan T. K., Kereš D., Oñorbe J., Hopkins P. F., Muratov A. L., Faucher-Giguère C.-A., Quataert E., 2015, MNRAS, 454, 2981
Chua K. T. E., Pillepich A., Rodriguez-Gomez V., Vogelsberger M., Bird S., Hernquist L., 2016, preprint (arXiv:1611.07991)
Conroy C., Wechsler R. H., Kravtsov A. V., 2006, ApJ, 647, 201
Cui W. et al., 2016, MNRAS, 458, 4052
D'Onghia E., Springel V., Hernquist L., Keres D., 2010, ApJ, 709, 1138
Dalal N., Kochanek C. S., 2002, ApJ, 572, 25
Despali G., Vegetti S., 2017, MNRAS, 469, 1997
di Cintio A., Knebe A., Libeskind N. I., Yepes G., Gottlöber S., Hoffman Y., 2011, MNRAS, 417, L74
Di Cintio A., Brook C. B., Macciò A. V., Stinson G. S., Knebe A., Dutton A. A., Wadsley J., 2014, MNRAS, 437, 415
El-Badry K., Wetzel A., Geha M., Hopkins P. F., Kereš D., Chan T. K., Faucher-Giguère C.-A., 2016, ApJ, 820, 131
Erkal D., Belokurov V., Bovy J., Sanders J. L., 2016, MNRAS, 463, 102
Errani R., Peñarrubia J., Laporte C. F. P., Gómez F. A., 2017, MNRAS, 465, L59
Fattahi A. et al., 2016, MNRAS, 457, 844
Faucher-Giguère C.-A., Lidz A., Zaldarriaga M., Hernquist L., 2009, ApJ, 703, 1416
Faucher-Giguère C.-A., Hopkins P. F., Kereš D., Muratov A. L., Quataert E., Murray N., 2015, MNRAS, 449, 987
Faucher-Giguère C.-A., Feldmann R., Quataert E., Kereš D., Hopkins P. F., Murray N., 2016, MNRAS, 461, L32
Feldmann R., Spolyar D., 2015, MNRAS, 446, 1000
Ferland G. J., Korista K. T., Verner D. A., Ferguson J. W., Kingdon J. B., Verner E. M., 1998, PASP, 110, 761
Fiacconi D., Madau P., Potter D., Stadel J., 2016, ApJ, 824, 144
Fillingham S. P., Cooper M. C., Wheeler C., Garrison-Kimmel S., Boylan-Kolchin M., Bullock J. S., 2015, MNRAS, 454, 2039
Fillingham S. P., Cooper M. C., Pace A. B., Boylan-Kolchin M., Bullock J. S., Garrison-Kimmel S., Wheeler C., 2016, MNRAS, 463, 1916
Fitts A. et al., 2016, preprint (arXiv:1611.02281)
Garrison-Kimmel S., Boylan-Kolchin M., Bullock J. S., Lee K., 2014a, MNRAS, 438, 2578
Garrison-Kimmel S., Boylan-Kolchin M., Bullock J. S., Kirby E. N., 2014b, MNRAS, 444, 222
Garrison-Kimmel S., Bullock J. S., Boylan-Kolchin M., Bardwell E., 2017, MNRAS, 464, 3108
Gnedin O. Y., Hernquist L., Ostriker J. P., 1999, ApJ, 514, 109
Governato F. et al., 2012, MNRAS, 422, 1231
Graus A. S., Bullock J. S., Boylan-Kolchin M., Weisz D. R., 2016, MNRAS, 456, 477
Griffen B. F., Ji A. P., Dooley G. A., Gómez F. A., Vogelsberger M., O'Shea B. W., Frebel A., 2016, ApJ, 818, 10
Gritschneder M., Lin D. N. C., 2013, ApJ, 765, 38
Hafen Z. et al., 2017, MNRAS, 469, 2292
Hahn O., Abel T., 2011, MNRAS, 415, 2101
Hargis J. R., Willman B., Peter A. H. G., 2014, ApJ, 795, L13
Hayashi E., Navarro J. F., Taylor J. E., Stadel J., Quinn T., 2003, ApJ, 584, 541
Hernquist L., 1990, ApJ, 356, 359
Hezaveh Y. D. et al., 2016, ApJ, 823, 37
Hirschmann M., De Lucia G., Wilman D., Weinmann S., Iovino A., Cucciati O., Zibetti S., Villalobos Á., 2014, MNRAS, 444, 2938
Hopkins P. F., 2015, MNRAS, 450, 53
Hopkins P. F., Narayanan D., Murray N., 2013, MNRAS, 432, 2647
Hopkins P. F., Kereš D., Oñorbe J., Faucher-Giguère C.-A., Quataert E., Murray N., Bullock J. S., 2014, MNRAS, 445, 581
Hopkins P. F. et al., 2017, preprint (arXiv:1702.06148)
Horiuchi S., Humphrey P. J., Oñorbe J., Abazajian K. N., Kaplinghat M., Garrison-Kimmel S., 2014, Phys. Rev. D, 89, 025017
Horiuchi S., Bozek B., Abazajian K. N., Boylan-Kolchin M., Bullock J. S., Garrison-Kimmel S., Onorbe J., 2016, MNRAS, 456, 4346
Hunter J. D., 2007, Comput. Sci. Eng., 9, 90
Ibata R. A., Lewis G. F., Martin N. F., 2016, ApJ, 819, 1
Jethwa P., Belokurov V., Erkal D., 2016, preprint (arXiv:1612.07834)
Johnston K. V., Spergel D. N., Haydn C., 2002, ApJ, 570, 656
Jones E., Oliphant T., Peterson P. et al., 2001–, SciPy: Open source scientific tools for Python. Available at: http://www.scipy.org/
Kamionkowski M., Liddle A. R., 2000, Phys. Rev. Lett., 84, 4525
Katz N., White S. D. M., 1993, ApJ, 412, 455
Kim J.-h. et al., 2014, ApJS, 210, 14
Klypin A., Kravtsov A. V., Valenzuela O., Prada F., 1999, ApJ, 522, 82
Knollmann S. R., Knebe A., 2009, ApJS, 182, 608
Koposov S. E., Rix H.-W., Hogg D. W., 2010, ApJ, 712, 260

Kroupa P., 2001, MNRAS, 322, 231
Krumholz M. R., Gnedin N. Y., 2011, ApJ, 729, 36
Kuhlen M., Diemand J., Madau P., 2008, ApJ, 686, 262
Kuhlen M., Madau P., Silk J., 2009, Science, 325, 970
Leauthaud A. et al., 2012, ApJ, 744, 159
Leitherer C. et al., 1999, ApJS, 123, 3
Ma X., Hopkins P. F., Faucher-Giguère C.-A., Zolman N., Muratov A. L., Kereš D., Quataert E., 2016, MNRAS, 456, 2140
Ma X., Hopkins P. F., Wetzel A. R., Kirby E. N., Anglés-Alcázar D., Faucher-Giguère C.-A., Kereš D., Quataert E., 2017, MNRAS, 467, 2430
MacLeod C. L., Jones R., Agol E., Kochanek C. S., 2013, ApJ, 773, 35
Mahajan S., Mamon G. A., Raychaudhury S., 2011, MNRAS, 416, 2882
Mao S., Schneider P., 1998, MNRAS, 295, 587
Mao Y.-Y., Williamson M., Wechsler R. H., 2015, ApJ, 810, 21
Mashchenko S., Wadsley J., Couchman H. M. P., 2008, Science, 319, 174
Miyamoto M., Nagai R., 1975, PASJ, 27, 533
Moore B., Ghigna S., Governato F., Lake G., Quinn T., Stadel J., Tozzi P., 1999, ApJ, 524, L19
Moster B. P., Naab T., White S. D. M., 2013, MNRAS, 428, 3121
Muratov A. L., Kereš D., Faucher-Giguère C.-A., Hopkins P. F., Quataert E., Murray N., 2015, MNRAS, 454, 2691
Muratov A. L. et al., 2017, MNRAS, 468, 4170
Navarro J. F., Frenk C. S., White S. D. M., 1996, ApJ, 462, 563
Newberg H. J., Carlin J. L. eds, 2016, Tidal Streams in the Local Group and Beyond Astrophysics and Space Science Library Vol. 420, doi:10.1007/978-3-319-19336-6.
Ngan W., Bozek B., Carlberg R. G., Wyse R. F. G., Szalay A. S., Madau P., 2015, ApJ, 803, 75
Ngan W., Carlberg R. G., Bozek B., Wyse R. F. G., Szalay A. S., Madau P., 2016, ApJ, 818, 194
Nierenberg A. M., Treu T., Wright S. A., Fassnacht C. D., Auger M. W., 2014, MNRAS, 442, 2434
Oman K. A., Hudson M. J., 2016, MNRAS, 463, 3083
Oñorbe J., Garrison-Kimmel S., Maller A. H., Bullock J. S., Rocha M., Hahn O., 2014, MNRAS, 437, 1894
Oñorbe J., Boylan-Kolchin M., Bullock J. S., Hopkins P. F., Kereš D., Faucher-Giguère C.-A., Quataert E., Murray N., 2015, MNRAS, 454, 2092
Papastergis E., Giovanelli R., Haynes M. P., Shankar F., 2015, A&A, 574, A113
Peñarrubia J., Benson A. J., Walker M. G., Gilmore G., McConnachie A. W., Mayer L., 2010, MNRAS, 406, 1290
Perez F., Granger B. E., 2007, Comput. Sci. Eng., 9, 21
Pontzen A., Governato F., 2012, MNRAS, 421, 3464
Price D. J., Monaghan J. J., 2007, MNRAS, 374, 1347
Quinn P. J., Hernquist L., Fullagar D. P., 1993, ApJ, 403, 74
Ramachandran P., Varoquaux G., 2011, Comput. Sci. Eng., 13, 40
Read J. I., Gilmore G., 2005, MNRAS, 356, 107
Read J. I., Wilkinson M. I., Evans N. W., Gilmore G., Kleyna J. T., 2006a, MNRAS, 366, 429
Read J. I., Wilkinson M. I., Evans N. W., Gilmore G., Kleyna J. T., 2006b, MNRAS, 367, 387
Reddick R. M., Wechsler R. H., Tinker J. L., Behroozi P. S., 2013, ApJ, 771, 30
Sanders J. L., Bovy J., Erkal D., 2016, MNRAS, 457, 3817
Sanderson R. E., Vera-Ciro C., Helmi A., Heit J., 2016, preprint (arXiv:1608.05624)
Sawala T. et al., 2015, MNRAS, 448, 2941
Sawala T. et al., 2016, MNRAS, 457, 1931
Sawala T., Pihajoki P., Johansson P. H., Frenk C. S., Navarro J. F., Oman K. A., White S. D. M., 2017, MNRAS, 467, 4383 (S17)
Schaye J. et al., 2015, MNRAS, 446, 521
Somerville R. S., 2002, ApJ, 572, L23
Springel V., 2005, MNRAS, 364, 1105
Springel V. et al., 2008, MNRAS, 391, 1685
Stadel J., Potter D., Moore B., Diemand J., Madau P., Zemp M., Kuhlen M., Quilis V., 2009, MNRAS, 398, L21
Su K.-Y., Hopkins P. F., Hayward C. C., Faucher-Giguere C.-A., Keres D., Ma X., Robles V. H., 2016, preprint (arXiv:1607.05274)
Taylor J. E., Babul A., 2001, ApJ, 559, 716
Teyssier M., Johnston K. V., Kuhlen M., 2012, MNRAS, 426, 1808
Tollerud E. J., Bullock J. S., Strigari L. E., Willman B., 2008, ApJ, 688, 277
Tollerud E. J., Boylan-Kolchin M., Bullock J. S., 2014, MNRAS, 440, 3511
van der Walt S., Colbert S. C., Varoquaux G., 2011, Comput. Sci. Eng., 13, 22
Vegetti S., Koopmans L. V. E., Bolton A., Treu T., Gavazzi R., 2010, MNRAS, 408, 1969
Vera-Ciro C. A., Helmi A., Starkenburg E., Breddels M. A., 2013, MNRAS, 428, 1696
Vogelsberger M. et al., 2014a, MNRAS, 444, 1518
Vogelsberger M. et al., 2014b, Nature, 509, 177
Wang J., Frenk C. S., Navarro J. F., Gao L., Sawala T., 2012, MNRAS, 424, 2715
Wetzel A. R., White M., 2010, MNRAS, 403, 1072
Wetzel A. R., Tinker J. L., Conroy C., van den Bosch F. C., 2013, MNRAS, 432, 336
Wetzel A. R., Tinker J. L., Conroy C., van den Bosch F. C., 2014, MNRAS, 439, 2687
Wetzel A. R., Deason A. J., Garrison-Kimmel S., 2015a, ApJ, 807, 49
Wetzel A. R., Tollerud E. J., Weisz D. R., 2015b, ApJ, 808, L27
Wetzel A. R., Hopkins P. F., Kim J.-h., Faucher-Giguère C.-A., Kereš D., Quataert E., 2016, ApJ, 827, L23
Yin J., Hou J. L., Prantzos N., Boissier S., Chang R. X., Shen S. Y., Zhang B., 2009, A&A, 505, 497
Yoon J. H., Johnston K. V., Hogg D. W., 2011, ApJ, 731, 58
Zentner A. R., Bullock J. S., 2003, ApJ, 598, 49
Zhu Q., Marinacci F., Maji M., Li Y., Springel V., Hernquist L., 2016, MNRAS, 458, 1559
Zolotov A. et al., 2012, ApJ, 761, 71

APPENDIX A: DISTRIBUTIONS WITHIN 50 AND 300 KPC

The figures presented in the main body of the paper plot subhalo counts, as a function of $V_{\rm max}$, $d_{\rm peri}$, and $V_{\rm tan}$, within 100 kpc. For completeness, we plot here similar distributions, but including subhaloes within either 50 kpc (Fig. A1) or 300 kpc (Fig. A2) of the host centres. The fractional difference in the purely DMO simulations is lower on ∼300 kpc scales than within either 50 or 100 kpc, but the impact of the central galaxy remains present in the lack of subhaloes with low $V_{\rm tan}$ or small $d_{\rm peri}$. Within 50 kpc, the central galaxy is extremely destructive: only ∼25 per cent of the subhaloes present in the DMO simulations survive in the presence of a disc. Similarly, no subhaloes with $V_{\rm tan} \lesssim 100\,{\rm km\,s^{-1}}$ remain within 50 kpc of the galaxy.

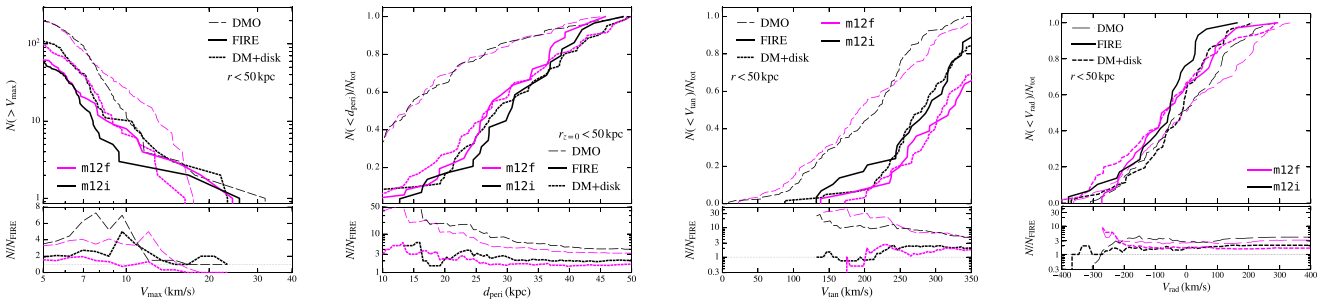

Figure A1. From left to right, cumulative counts of subhalo within 50 kpc, as a function of $V_{\rm max}$ (similar to the top panels of Fig. 2); normalized counts as a function of pericentric distance (similar to the left-hand panel of Fig. 5); and normalized counts as a function of tangential and radial velocity (similar to Fig. 6). All trends are similar to those presented in the main text: subhaloes on radial orbits (low $V_{\rm tan}$ and small $d_{\rm peri}$) are readily destroyed. However, the overall destruction is higher within 50 kpc: DMO simulations overpredict the total number of subhaloes by a factor of 3–4, compared to factors of 1.5–2 within 100 kpc.

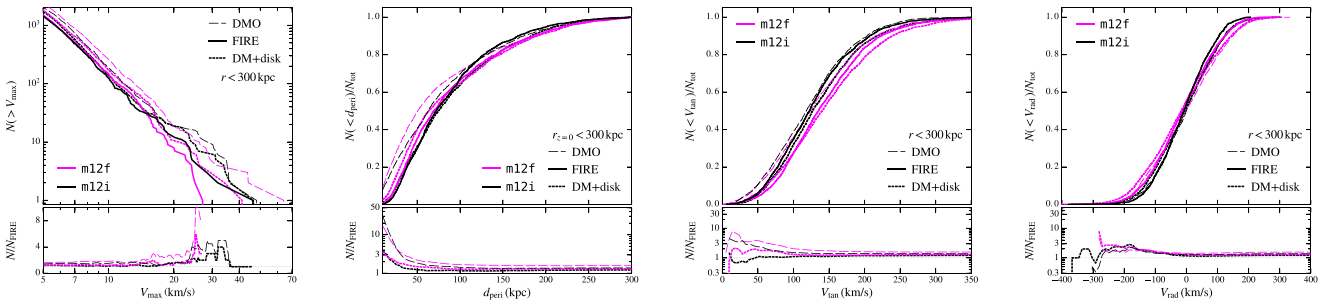

Figure A2. Identical to Fig. A1, but including all subhaloes within 300 kpc, roughly corresponding to the host haloes' virial radii. The relative amount of destruction is significantly lower than within 50 or 100 kpc, but the embedded disc simulations still yield a better match than the DMO simulations to the FIRE baryonic simulations. Moreover, the imprint of the central galaxy remains on the $d_{\rm peri}$ and $V_{\rm tan}$ distributions, even out to 300 kpc.

APPENDIX B: RESOLUTION

Because of the cost of simulating the systems at even higher resolution than that presented in the main body, we instead establish that we reliably identify substructures at the same particle count using lower-resolution simulations. Specifically, we compare counts as a function of mass and radius to simulations of `m12i` with particle masses 8 times larger than our fiducial simulations ($m_{\rm p} = 3.4 \times 10^5\,{\rm M}_\odot$) and with softening lengths a factor of 2 larger. A detailed discussion of resolution in the FIRE simulations can be found in Hopkins et al. (2017).

The left-hand panel of Fig. B1 shows cumulative counts as a function of bound mass assigned by `AHF`, M, within 100 kpc of `m12i`, corrected for $f_{\rm b}$. The black lines present counts in simulations with the fiducial disc parameters, while the brown lines plot the DMO counterparts; fiducial resolution simulations are plotted in solid, and those at lower resolution are dashed. The lower sub-panel shows the ratio between the low- and high-resolution versions of the run with and without the disc. The dotted vertical line represents the resolution cut of $3 \times 10^6\,{\rm M}_\odot \sim 85$ particles adopted in the main text based on inspection of the differential mass functions. The dashed vertical line indicates a factor of 8 larger mass, corresponding to an identical number of particles in the lower resolution simulation ($M = 2.4 \times 10^7\,{\rm M}_\odot$, after multiplying by $1 - f_{\rm b}$). Counts in the disc simulations agree well at that mass (though there are fluctuations at higher mass), and counts in the DMO simulations only differ by ∼15 per cent. Convergence is generally even better on larger scales: counts agree to within 10 per cent at nearly all $M > 2.4 \times 10^7\,{\rm M}_\odot$. The low-resolution DMO simulation does, however, underpredict the subhalo count within 300 kpc by ∼10 per cent, and only agrees for ∼300 particles; at that particle count, however, the low-resolution disc simulation *overpredicts* the subhalo count by ∼10 per cent.

The right-hand panel of Fig. B1 shows the radial distribution of subhaloes with $M > 2.4 \times 10^7\,{\rm M}_\odot$ in the same four simulations. Counts in the disc runs agree to within a few per cent at nearly all radii, and the DMO simulations are within ∼10–15 per cent of one another. The offset in the latter is roughly constant with radius, indicating that the deficiency discussed above is relatively independent of distance. The most significant deviations occur at $r \lesssim 40$ kpc or $M > 3 \times 10^8\,{\rm M}_\odot$, where the number of subhaloes is small (<10) and therefore subject to significant scatter, depending the subhaloes' orbital phases. In general, the differences between the resolution levels are small compared to the differences between the DMO and disc simulations.

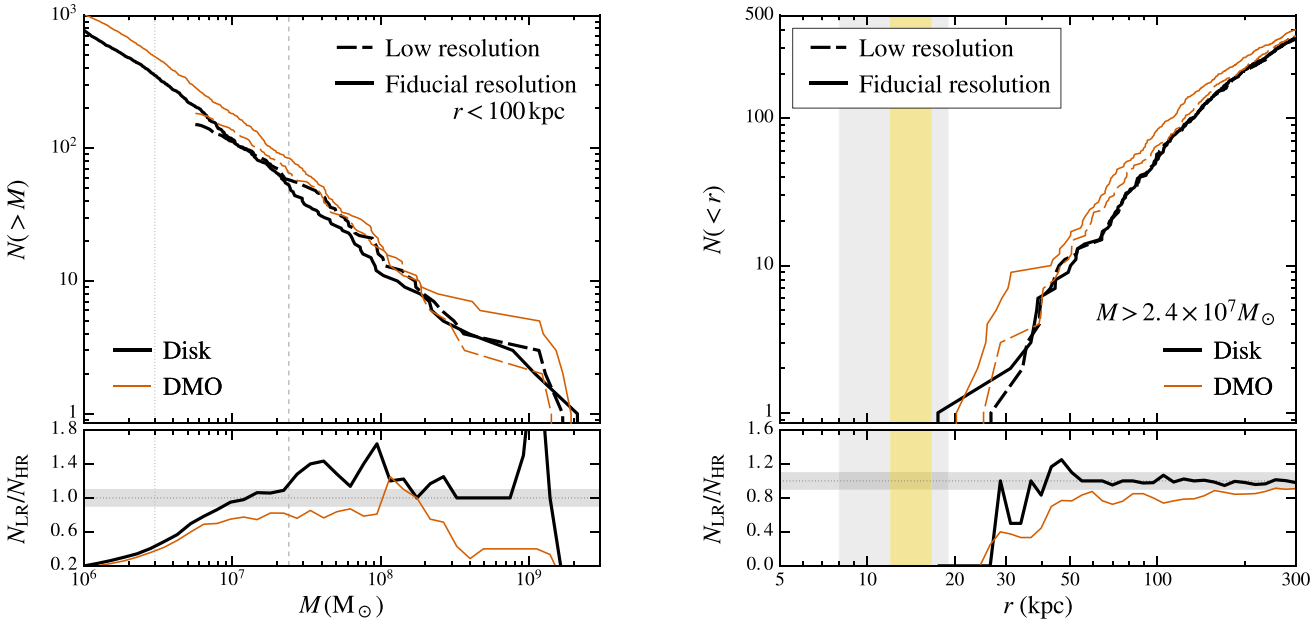

Figure B1. Comparing subhalo counts at our fiducial (high) resolution (solid lines) to those in a low-resolution simulation with 8× fewer particles (dashed lines). The black curves show the DM only (DMO) simulations while the orange curves show the simulations with an embedded disc. The left-hand panel shows the cumulative number of subhaloes above a given subhalo bound mass, M, within 100 kpc. We correct M for the baryon fraction. The dotted vertical line at 3×10^6 $M_\odot$ shows the resolution cut used in Figs 3–6; the dashed vertical line shows an equivalent number of particles in the low-resolution simulation, $M = 2.4 \times 10^7$ $M_\odot$. As demonstrated by the lower panel, which plots the ratio of subhalo counts in the low- and high-resolution simulations, the counts are converged to within ∼15 per cent at that particle count. The shaded band indicates ±10 per cent. The right-hand panel demonstrates that counts of subhaloes above this mass are also well converged as a function of radius: the embedded disc simulations agree to within a few per cent at nearly all radii, and the relatively flat offset in the DMO run is consistent with the underprediction discussed in the text. The most significant deviations occur at $r \lesssim 40$ kpc or $M > 3 \times 10^8$ $M_\odot$, where the number of subhaloes is small (<10) and therefore subject to significant scatter.

This paper has been typeset from a TEX/LATEX file prepared by the author.